UNIVERSITY POLITEHNICA OF BUCHAREST
Doctoral School of Energy Engineering
Hydraulics, Hydraulic Machinery and Environmental Engineering Department

CONTRIBUTIONS ON THE BOUNDARY LAYER FLOW NUMERICAL MODELLING IN TURBULENT REGIME

< Thesis Summary >

Author: Ionuț Stelian GRECU

Scientific Supervisor: Conf. dr. ing. Diana Maria BUCUR

UPB, 2023

THESIS SUMMARY CONTENT

THESIS CONTENTS

KEYWORDS

Computational Fluid Dynamics, CFD, Direct Numerical Simulations, DNS, Large Eddy Simulations, LES, Reynolds Averaged Navier Stokes, RANS, Reynolds Stress Model, RSM, Shear Stress Transport, SST, Unsteady Reynold Averaged Navier Stokes, URANS, steady-state flow, unsteady-state flow, pulsating flow, turbulence modelling, boundary layer, oscillating layer, pressure gradient, k-ε turbulence model, k-ω SST turbulence model, standard wall function, Manhart wall model, Duprat wall model.

SCIENTIFIC ACTIVITY

Published papers:

1. **I. S. Grecu**, G. Dunca, D. M. Bucur and M. J. Cervantes, "Wall-Layer Treatment Considering the Pressure Gradient for RANS Simulations of Turbulent Flows," *2019 International Conference on ENERGY and ENVIRONMENT (CIEM)*, Timisoara, Romania, **2019**, pp. 289-293, doi: 10.1109/CIEM46456.2019.8937633.
2. **I. S. Grecu**, D. M. Bucur, G. Dunca, V. N. Panaitescu and M. J. Cervantes, "Implementation of the standard wall function in numerical computation software," *2017 International Conference on ENERGY and ENVIRONMENT (CIEM)*, Bucharest, Romania, **2017**, pp. 231-235, doi: 10.1109/CIEM.2017.8120848.
3. G. Dunca, D. M. Bucur, R. Gabriela Iovănel, C. Călinoiu, **I. S. Grecu** and R. Mitruț, "Efficiency Evaluation and Vibration Analysis of Small Pelton Turbines," *2019 International Conference on ENERGY and ENVIRONMENT (CIEM)*, Timisoara, Romania, **2019**, pp. 384-388, doi: 10.1109/CIEM46456.2019.8937612.
4. S. Năstase, C. -G. Andrei, E. I. Tică, S. -C. Georgescu, A. Neagoe and **I. S. Grecu**, "Hydropower Optimization Test-Case Solved with Nature-Inspired Algorithms," *2019 International Conference on ENERGY and ENVIRONMENT (CIEM)*, Timisoara, Romania, **2019**, pp. 244-248, doi: 10.1109/CIEM46456.2019.8937643.
5. **I. S. Grecu**, G. Dunca, D. M. Bucur, and M. J. Cervantes, "URANS numerical simulations of pulsating flows considering streamwise pressure gradient on asymmetric diffuser," *IOP Conference Series: Earth and Environmental Science*, vol. 1079, no. 1, p. 012087, Sep. **2022**, doi: 10.1088/1755-1315/1079/1/012087.
6. **I. S. Grecu**, G. Dunca, D. M. Bucur and M. J. Cervantes, "Wall-Model for Turbulent Flows Under an Adverse Pressure Gradient - Asymmetric Diffuser," *2021 10th International Conference on ENERGY and ENVIRONMENT (CIEM)*, Bucharest, Romania, **2021**, pp. 1-5, doi: 10.1109/CIEM52821.2021.9614830.
7. D. M. Bucur, G. Dunca, F. Bunea, R. A. Chihaia, **I. S. Grecu**, and R. Mitruț, "Experimental investigation of small axial hydro-kinetic turbines," *IOP Conference Series: Earth and Environmental Science*, vol. 1079, no. 1, p. 012020, Sep. **2022**, doi: 10.1088/1755-1315/1079/1/012020.
8. D. M. Bucur, **I. S. Grecu**, R. Mitruţ, C. Drăgoi, A. -I. Stroilescu and G. Dunca, "Design and Numerical Investigation of a Small Axial Hydrokinetic Turbine," *2021 10th International Conference on ENERGY and ENVIRONMENT (CIEM)*, Bucharest, Romania, **2021**, pp. 1-5, doi: 10.1109/CIEM52821.2021.9614895.
9. P. Danca, F. Bunea, C. Babutanu, A. Nedelcu, and **I. S. Grecu**, "Experimental study of the flow induced by an axial hydrokinetic turbine," IOP Conference Series: Earth and Environmental Science, vol. 1136, no. 1, p. 012058, Jan. **2023**, doi: 10.1088/1755-1315/1136/1/012058.

10. R. Roman, R. Iovanel, **I. S. Grecu**, G. Dunca, and D. Bucur, "EXPERIMENTAL EVALUATION OF ROUGHNESS COEFFICIENT OF A HPP HEADRACE CHANNEL," *U.P.B. Sci. Bull., Series D*, vol. 77, no. 3, **2015**. Available: https://www.scientificbulletin.upb.ro/rev_docs_arhiva/fullf90_304489.pdf

Member in research projects

1. **i-TURB** sistem integrat pentru obținerea celui mai bun echilibru între potențialul ecologic al apei și eficiența turbinei, **2022 – 2024**
2. Producerea energiei la baraje existente fără folosință energetică, **EEA AND NORWAY GRANTS FROM INNOVATION NORWAY**, Marcel Istrate (manager proiect, Universitatea Tehnică Gh. Asachi din Iași), Bucur D.M. (responsabil partener P1, Universitatea Politehnica din București), **2022-2023**
3. **HyPER -** Ecological energy system for the use of hydrokinetic energy of very low water streams, **2020 – 2022**
4. **ECOTURB -** Sistem inovativ de aerare a apei turbinate în vederea menținerii condițiilor necesare vieții acvatice, **2014 – 2017**
5. Influența parametrilor dinamici ai curgerii asupra evaluării debitului în metoda presiune-timp, Grant intern UPB, **2016 – 2017**
6. Schimburi ionice în acvifere, Grant intern UPB, **2017 – 2018**
7. Intelligent Energetic System in Protected Areas (SEI), EEA Grants, **2015 – 2017**

INTRODUCTION

The fast increase in the energy production from renewable energy sources, mainly solar Photovoltaics (PV) and wind, is encouraged resulting into a healthy green environment. However, because the production of energy from the solar PV and wind renewable energy sources cannot be predicted, they can disrupt the stability of the electrical grid system. According to the International Energy Agency (IEA) 2022 report [1] in 2019 the energy production increased from solar PV and wind sources by 11.6 % and 35.7 % respectively and as a result the stability of the electrical grid system was strongly affected. In this context, hydropower energy plays an essential role in the stability of the electrical grid system as water is the only one capable of being stored at a large scale on the long term.

Each time a hydraulic turbine is operated under different loads than the rated one or during load variations, it is subjected to hydraulic and mechanical overloads leading to shortening the lifetime of the turbines components [2], [3]. To lower the financial and time resources for assessing the turbine performances, a great interest in computational fluid dynamics (CFD) is rising. The numerical simulation approach can be used to design and estimate the turbine performances in a cost-effective manner [4], [5]. In most industrial applications, the Reynolds Averaged Navier Stokes (RANS) equations-based turbulence models are used, due to their small computational requirements [6], [7]. Over time, different wall treatments were developed for the RANS equations-based turbulence models with the purpose of a better estimation of the flow quantities in the near wall zone. Over the past decade, special attention was given to modifying the turbulence models with different sets of equations and algorithms, with the purpose of improving the simulations results or simply to reduce the required time and/or computational power requirements, by observing other flow characteristics that can be taken into consideration such as the pressure gradient [8], [9]. To improve the solution of the RANS numerical simulations, the k - ω turbulence model was developed. The use of this model requires a very fine discretization of the computational grid, with $y^+ = 1$, leading to large time and computational effort [4], [7].

The work of the thesis is focused around the two equations eddy viscosity turbulence model, the k - ω turbulence model. The main reason for choosing the eddy viscosity turbulence models was that they represent the most used numerical approaches in the academic community and in the industry [6], [7]. Two wall models are used for implementation, one developed by Manhart [8], and one by Duprat [10]. The two wall models were developed based on the standard wall function and, in addition, they consider the influence of the streamwise pressure gradient [8], [10]. So far, the wall models were successfully validated against Direct Numerical Simulations (DNS), by Manhart [8] and Duprat [10], and Large Eddy Simulations (LES) by Duprat [10]. In this thesis, the Manhart and Duprat wall models, were implemented in the k - ω SST turbulence model used to carry out RANS numerical simulations of steady flow and unsteady pulsating turbulent flows.

The ***main objective*** of this thesis is to decrease the computation time and computational effort of numerical simulations using wall models in flows with strong adverse pressure gradients and pulsations. The wall models used in the numerical simulations are the standard formulation of the k - ω SST turbulence model (linear law of the wall), the Manhart wall model [8] and the Duprat wall model [11]. The wall models of Manhart and Duprat are implemented in the k - ω SST turbulence model. The RANS numerical simulations performed are steady-state and unsteady-state numerical simulations. The unsteady-state numerical simulations are carried out to resemble several pulsating turbulent flows. The turbulent flows analysed are characterized by three oscillations frequencies 0.03 Hz, 0.10 Hz, 0.35 Hz. The results of the numerical simulations showed a decrease in the computation time and computational effort

required while keeping a good approximation of the experimental measurements. The test case on which the numerical simulations are performed replicates the experimental set-up of Cervantes and Engström [12] which is also used for validation.

In this thesis investigations are conducted to study the work of Manhart and Duprat on more complex geometries and flow regimes. The wall models of Manhart and Duprat were used in numerical simulations performed on an asymmetric diffuser for one steady flow and three pulsating flows. The Manhart and Duprat wall models are applied to RANS based numerical simulations in contrast to the DNS and LES analysis conducted by Manhart and Duprat. The first two chapters present the state of the art of flow analysis in CFD, where the usual wall functions and turbulence models are used in CFD. Also, in these chapters the wall models of Manhart and Duprat are presented. In chapter 3 the free open source CFD code, Code_Saturne, is presented followed by the wall functions implementation procedure. Chapters 4 and 5 presents the experimental and numerical test cases followed by the experimental data processed for validating the numerical simulations of the steady and three pulsating flows. The comparisons between the experimental data and the numerical simulations are presented in chapter 6 for steady flow and in chapter 7 for pulsating flows, including the sensitivity analyses of each type of numerical simulation. At the end of the thesis are presented the conclusions, personal contributions and future work directions of the research conducted.

THEORETICAL ASPECTS OF TURBULENT BOUNDARY LAYER IN CFD

Turbulent flows involve high Reynolds numbers, that contain 3D fluid structures known as eddies or vortices. The eddies inside the turbulent flows are present in a wide range of sizes that are randomly changing in both time and space. Modelling the turbulence requires the estimation of all eddies energy, from the smallest to the largest one, in both time and space, resulting in a very difficult task to accomplish. However, numerous efforts have been made in predicting the turbulence using different models and numerical approaches [13], [14], [15], [16], [17], [18].

The first approach is the Direct Numerical Simulations (DNS). It is the most accurate numerical method in which the Navier-Stokes equations, (1) and (2), are solved for all structures in the turbulent flow. The disadvantage of DNS is that the computational power requirement is extremely high, and a very fine mesh must be made. The computational effort for using DNS is increased with the Reynolds number (Re) the number of mesh node is proportional to Re^3 [7]. Therefore, making its availability of use limited to geometries with low or moderate Reynolds number flows [7], [4], [19], [20].

$$\frac{\partial \rho}{\partial t} + \nabla \cdot \left(\rho \underline{u} \right) = 0 \tag{1}$$

$$\frac{\partial \left(\rho \underline{u} \right)}{\partial t} + \nabla \cdot \left(\rho \underline{u} \otimes \underline{u} \right) = -\nabla P + \nabla \cdot \left(\overline{\overline{\tau}} \right) + \rho \underline{g} \tag{2}$$

The second approach is the Large Eddy Simulations (LES). It gives a very good estimation of the turbulent flow while demanding less computational effort than the DNS approach. The LES method solves only a part of the turbulent motions inside the fluid, that is the large scales, or the large eddies, using a "filtered" velocity field defined as a function of length and time dependent, $\tilde{U}(x, t)$ [21]. In LES, a modified version of the Navier-Stokes equations, (1) and (2), is solved only for the large motions scales, while for the rest of the motion scales includes a model that considers the influence of the small eddies from the fluid.

The third approach is the Reynolds-Averaged Navier-Stokes (RANS) simulations. This approach uses turbulence models for predicting the motions in the turbulent flow. It is

economical in terms of computational power requirement, where very fine mesh and direct calculation of the Navier-Stokes equations can be avoided [7], [6]. The RANS approach solves the Navier-Stokes equations using the Reynolds-averaged method. It is based on using a statistical approach, (3), where the instantaneous quantities of the flow, ϕ, are decomposed into a time-averaged component, $\bar{\phi}$, and a time-fluctuating component, ϕ', [7], [6], [22], [23].

$$\phi(x,t) = \bar{\phi}(x) + \phi'(x,t) \tag{3}$$

where ϕ is the instantaneous variable, $\bar{\phi}$ - the time-averaged variable component, ϕ' - the time-fluctuating part of the variable.

The application of the Reynolds-averaged method over the non-linear Navier-Stokes equations results in additional terms that need to be modelled. The additional unknown terms are called Reynolds stresses, R_{ij}, and they are determined using turbulence models. These turbulence models contain equations used for calculating the Reynolds stresses, e.g., the *k-ε* turbulence model, the *k-ω* turbulence model etc. [7], [6], [23], [24].

The most frequently used turbulence models are the two-equations turbulence models: the standard *k-ε* turbulence model and the *k-ω* SST turbulence model. In addition to the continuity and momentum equations two more equations are added: one equation for the turbulent kinetic energy, *k*, and depending on the turbulence model used, another equation for the turbulence dissipation rate, *ε*, or the specific dissipation rate of turbulent kinetic energy, *ω*, also known as the turbulence frequency [7], [22], [23], [24].

The *k–ω* SST turbulence model

The k–ω SST turbulence model is based on the k-ω turbulence model, equations (4) and (5), combined with the advantages of the *k-ε* turbulence model. Therefore, it offers accurate results both in the near-wall region and further from the wall. In the near-wall region, where the flow separation occurs due to adverse pressure gradients and geometries with strong curvatures, the *k-ω* SST turbulence model uses the *k-ω* turbulence model formulation. Far from the near-wall region, the *k-ω* SST turbulence model behaves as the *k-ε* turbulence model in the modelling the flow. To use the proper turbulence model formulation for either near-wall region or for the region far away from the wall, the *k-ω* SST turbulence model involves the use of blending functions.

The transport equations used for the *k-ω* turbulence model are:

$$\frac{\partial}{\partial t}(\rho k) + \frac{\partial}{\partial x_i}(\rho k \underline{u}) = \frac{\partial}{\partial x_j}\left[\left(\mu + \frac{\mu_t}{\sigma_k}\right)\frac{\partial k}{\partial x_j}\right] + P_k - \beta'\rho k\omega + P_{kb} \tag{4}$$

$$\frac{\partial}{\partial t}(\rho \omega) + \frac{\partial}{\partial x_i}(\rho \omega \underline{u}) = \frac{\partial}{\partial x_j}\left[\left(\mu + \frac{\mu_t}{\sigma_\omega}\right)\frac{\partial \omega}{\partial x_j}\right] + \alpha\frac{\omega}{k}P_k - \beta\rho\omega^2 + P_{\omega b} \tag{5}$$

where P_k is the production of turbulent kinetic energy and is calculated in the same way as for the *k-ε* turbulence model, $P_{\varepsilon b}$ is the production term due to buoyancy forces.

The constants of the *k-ω* turbulence model are presented in Table 1.

Table 1 Constants of the *k–ω* turbulence model

β	β'	α	σ_k	σ_ω
0.075	0.09	5/9	2	2

To consider the transport of the turbulent shear stress, a modification to the turbulent viscosity, μ_t, is required, as presented in equation (6) [23], [24].

$$\mu_t = \rho \frac{a_1 k}{\max\left(a_1 \omega; SF_2\right)} \tag{6}$$

$$F_2 = \tanh\left[\left(\max\left(\frac{2\sqrt{k}}{\beta' \omega y}; \frac{500\nu}{\omega y^2}\right)\right)^2\right] \tag{7}$$

where, a_1 is a model constant, with $a_1 = 0.31$, S is the invariant measure of the strain rate, F_2 is a blending function for calculations in the boundary layer.

The definition of the production term for the specific dissipation rate of turbulent kinetic energy, P_ω, is presented in equation (8).

$$P_\omega = \left(\frac{\alpha_3}{\nu_t}\right) P_k \tag{8}$$

Turbulent boundary layer modelling

- Standard wall function

It is based on the work of Launder and Spalding (1972) where the near-wall region can be divided in three sub-layers, Figure 1. The subdivisions of the near-wall region are delimited by the dimensionless distance normal to the wall, y^+, defined in equation (9) [7], [6], [24].

$$y^+ = \frac{y u_\tau}{\nu} \tag{9}$$

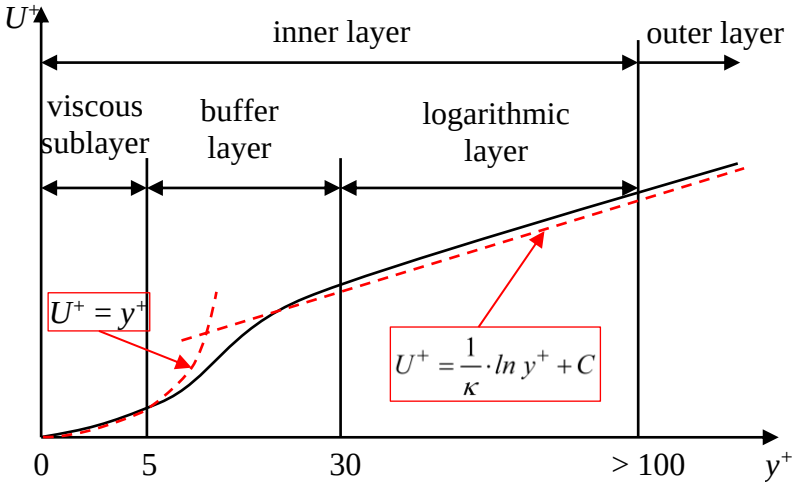

Figure 1. Subdivisions of the boundary layer in standard wall function

The "*viscous sublayer*" is limited to $y^+ \leq 5$ and in this region the velocity distribution is assumed to have a linear variation. The "*buffer layer*" starts from $y^+ = 5$ and it stops at around $y^+ = 30$. Here, because multiple forces are dominant over the velocity field, i.e., viscous and turbulence forces, it is very difficult to accurately predict the flow quantities inside the layer. The third layer of the boundary layer is called the "*logarithmic layer*" due to the velocity distribution that follows a logarithmic variation (known also as the *"log-law"*). The logarithmic layer usually starts from $y^+ = 30$ and it goes up to $y^+ = 100$, or even more, depending of the flow regime, [7], [22], [23], [24].

The velocity distribution used in the standard wall function is defined using the equation (10) for a $y^+ \leq 5$ and using the equation (11) for a $y^+ \geq 30$ [23].

$$U^+ = y^+ \tag{10}$$

$$U^+ = \frac{1}{\kappa}\ln y^+ + C \tag{11}$$

The formula of the friction velocity, u_τ, based on the wall shear stress is presented in equation (12).

$$u_\tau = \sqrt{\frac{\tau_w}{\rho}} \tag{12}$$

- Manhart wall model

Manhart [8] proposed a *new velocity scaling* that considers the pressure gradient in addition to the wall shear stress. For estimating the velocity field Manhart use a characteristic velocity, $u_{\tau p}$, instead of the friction velocity, u_τ, and it is based on the wall shear stress and the streamwise pressure gradient (Simpson [25]).

The characteristic velocity, $u_{\tau p}$, is defined as

$$u_{\tau p} = \sqrt{u_\tau^2 + u_p^2} \tag{13}$$

where, u_τ is the friction velocity due to the wall shear stress influence, equation (14),

$$u_\tau = \sqrt{\frac{\tau_w}{\rho}} \tag{14}$$

and u_p is the velocity influenced by the streamwise pressure gradient. equation (15).

$$u_p = \left|\frac{\mu}{\rho^2}\frac{\partial P}{\partial x}\right|^{1/3} \tag{15}$$

where, $\partial P / \partial x$ is the streamwise pressure gradient.

The wall model proposed by Manhart estimates the velocity profile for the "*viscous sublayer*", up to $y^+ = 5$, in dimensionless form, equation (16), using the equations (17).

$$U^* = sign(\tau_w)\alpha_m y^* + sign\left(\frac{\partial P}{\partial x}\right)(1-\alpha_m)^{3/2}\, y^{*2} \tag{16}$$

$$U^* = \frac{\bar{u}}{u_{\tau p}}; \quad y^* = \frac{y u_{\tau p}}{\nu}; \quad \alpha_m = \frac{u_\tau^2}{u_{\tau p}^2} \tag{17}$$

where y^* is the dimensionless distance based on the characteristic velocity defined in equation (13) and α_m is a parameter that takes account of wall shear stress, equation (14), and streamwise pressure gradient, equation (15).

Manhart validated his wall model results against DNS results. Due to the lack of computational power availability, the Manhart wall model was validated up to a $y^+ = 5$ [8].

- Duprat wall model

The Manhart wall model was further developed by Duprat [11] envisaging the accuracy improvement of the wall model and the application domain extension. The application domain of the Duprat wall model was extended compared to the Manhart wall model, from a $y^+ = 5$ up to $y^+ = 100$ [9], [11], [26].

To consider the pressure gradient further away from the wall, Duprat [11] developed a new turbulent viscosity, ν_t, model presented in equation (18). It is influenced by the two velocity scales, u_τ and u_p, the dimensionless wall normal distance, y^*, and the Kármán constant, κ.

$$\frac{\nu_t}{\nu} = \kappa y^* \left(\alpha_m + y^* \left(1-\alpha_m\right)^{3/2} \right)^{\beta_d} \left(1 - e^{-\frac{y^*}{1+A\alpha_m{}^3}} \right)^2 \tag{18}$$

where, β_d = 0.78 and A = 17, are two coefficients used in the Duprat wall model for approximation of the turbulent viscosity, ν_t, when compared to the DNS results, for a turbulent flow [11].

Using the turbulent viscosity equation (18), the Manhart wall model, equation (16), was developed by Duprat resulting in Duprat wall model, equation (19).

$$\frac{\partial U^*}{\partial y^*} = \frac{sign\left(\tau_w\right)\alpha_m + sign\left(\frac{\partial P}{\partial x}\right)\left(1-\alpha_m\right)^{3/2} y^*}{1+\kappa y^* \left(\alpha_m + y^* \left(1-\alpha_m\right)^{3/2} \right)^{\beta_d} \left(1 - e^{-\frac{y^*}{1+A\alpha_m{}^3}} \right)^2} \tag{19}$$

The validation procedure of the Duprat wall model was made using LES on test cases under the effects of the favourable or adverse pressure gradient where the y^+ reached values around 100 [9], [26].

The Duprat and Manhart wall models are working as a one scale velocity wall function, where the characteristic velocity scale, $u_{\tau p}$, is used which includes the influence of wall shear stress and streamwise pressure gradient. The characteristic velocity scale, $u_{\tau p}$, is based on the friction velocity, u_τ, and the velocity due to the pressure gradient, u_p, and the influence of the pressure gradient is accounted by a flow parameter, α.

CFD code Code_Saturne

Code_Saturne is an open-source software used for Computational Fluid Dynamics (CFD) applications, developed by EDF R&D. It can solve the Navier-Stokes equations for flow simulations in 2D or 3D dimensions for laminar or turbulent regime. Code_Saturne can solve the general flow equations for incompressible or weakly dilatable, steady or unsteady flows, using structured and unstructured meshes. Code_Saturne is compatible with several mesh generators software as: SALOME, Gambit, ICEM-CFD, Star-CCM+ etc. [23]. The code can also conduct numerical analyses based on several modules as: Lagrangian, Gas combustion module, Compressible module etc. The available simulation types for numerical analyses are the RANS-based simulations and the Large-Eddy Simulations, with various turbulence models options.

Code_Saturne uses a discretization based on a co-located Finite Volume approach, where the equations solved are integrated over each cell of the mesh domain or over the control volume Ω_i. Code_Saturne can carry out steady-state or unsteady-state numerical simulations. For the unsteady-state numerical simulations, Code_Saturne uses a θ-scheme for the discretization of time. It involves applying an algorithm based on a prediction-correction method to solve the mass and momentum equations. For pressure-velocity coupling Code_Saturne can use several algorithms as SIMPLE, SIMPLEC and PISO. Code_Saturne can solve the convective term using several schemes as Upwind, Centred and Second Order Linear Upwind (SOLU) Schemes. The SOLU scheme has the advantage of an increased precision

compared to the first two schemes. In Code_Saturne, two algorithms are available for computing the cell gradient for scalars and vector fields: the standard method and the Least-square method. Comparing the two methods, the standard method is more robust, but the computational effort is higher, while on the other hand the Least-square method is faster, but the results are less accurate.

Wall function implementation

A user defined wall function can be implemented in Code_Saturne using two methods, depending on the required level of detail:

1. The standard user boundary conditions, where to the standard boundary conditions of the domain can be applied simple mathematical expressions.

The standard boundary conditions can be modified through the Graphical User Interface (GUI) using the available built-in options or through simple user defined functions, as in equation (20).

$$U = 2 + \sin\left(a + b \cdot t\right) \tag{20}$$

where *a*, *b* and *t* are examples of several variables needed for the standard boundary condition.

2. The wall function boundary conditions, where advanced specific code language knowledge of Code_Saturne and several codes programming languages are required.

The user defined wall function boundary conditions require accessing the internal code variables used to either set the boundary conditions in a more advanced approach than the user law approach or to change the variation of the flow parameters inside the boundary layer.

The Duprat and Manhart wall models are implemented as a wall function boundary condition. A workflow diagram on how the Duprat or Manhart wall models are integrated in the Code_Saturne solver is presented in Figure 2, the location in the Code_Saturne computation process is marked with a red dotted contour. At the start of the numerical simulation the script with the simulation setup is passed to the kernel of Code_Saturne along with the pre-processor data, where the mesh is analysed and prepared for computation.

Code_Saturne handles the user-defined functions in two steps. In the first step, a verification of the user-defined function is made. This step is taking place at the start of the computational process where the user-defined functions are compiled into the code as an external input file. The second step is when the user-defined functions are applied to the computation process, after the mass and momentum equations are solved, red dotted line contour in Figure 2.

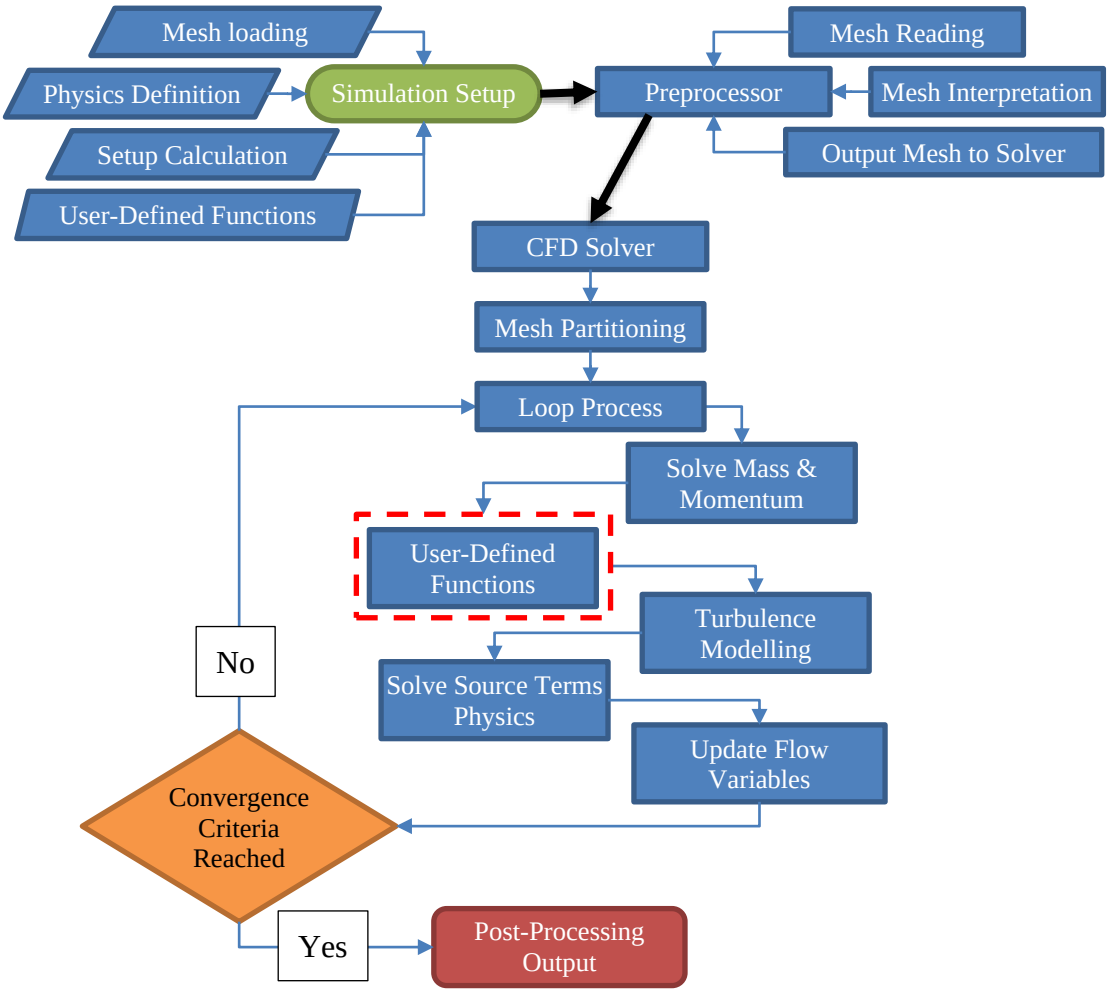

Figure 2. Integration of wall functions in Code_Saturne code.

ASYMMETRIC DIFFUSER NUMERICAL TEST CASE

The test case used in this thesis is an asymmetric diffuser preceded by a rectangular duct, Figure 3; see Cervantes and Engström [12]. The reason for using the experimental setup from the work of Cervantes and Engström [12] is the detailed velocity measurements performed in the boundary layer, under the influence of a moderate pressure gradient, making possible the validation of the numerical results against the experiments.

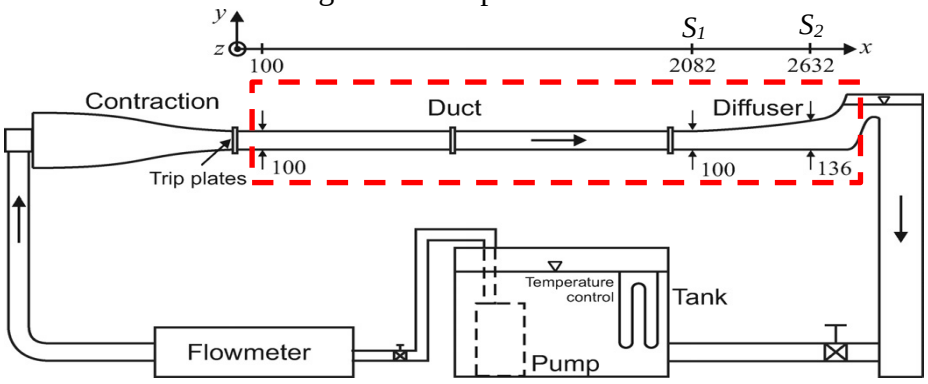

Figure 3. Experimental setup – asymmetric diffuser, dimensions in mm [12].

The test section used for the numerical analysis comprises of a straight rectangular duct of 2.102 m length, with a height h = 0.1 m and a width w = 0.15 m, followed by an asymmetric

rectangular diffuser with a diverging upper wall (Figure 3). The asymmetric diffuser from the experimental setup (Figure 3) was designed to maintain a constant adverse (or positive) pressure gradient on the entire length of the diffuser. It starts with an angle of 2.5° at the inlet, at x = 2.082 m, and increases smoothly, along the diffuser length, to an angle of 7.5° at the outlet, at x = 2.772 m, with an opening of 0.15 m × 0.15 m. The walls of the test section were made from transparent Plexiglas [12], [13].

The velocity measurements for this test case were carried out by Cervantes and Engström [12] using a Laser Doppler Anemometer (LDA). Experimental data of streamwise (in x-direction) and normal (in y-direction) velocity components, U and V, were measured at the bottom wall of the diffuser. During the analysed flow regimes, the two components of the velocity profile were measured in detail at two sections in the diffuser, at x = 2.082 m, S_1, and x = 2.632 m, S_2. The two measurement sections were chosen to analyse the flow with and without the influence of the adverse pressure gradient. The measurements were made at the half-width of the diffuser, z = 0.075 m, along a normal line from the bottom wall of the diffuser. The experiment was made for one steady-state regime and three unsteady-state regimes (pulsating flows) obtained by modifying the frequency of the pump electric current. The oscillations of the three pulsating flows are characterized on three frequencies f = 0.03 Hz, f = 0.10 Hz and f = 0.35 Hz. All the measurements made on the experimental setup were made with a maximum uncertainty of 0.5% for the velocity measurements [12].

Numerical test case

The geometry of the numerical test case comprises the straight rectangular duct, starting at x = 0.1 m, followed by the asymmetric diffuser, up to x = 2.772 m, as presented in Figure 3 marked with red discontinued line. The dimensions of the experimental setup are considered in designing the geometry for the numerical simulations. The geometry used for the numerical simulations is presented in Figure 4 and in Figure 5 is presented a detailed view on the diffuser part.

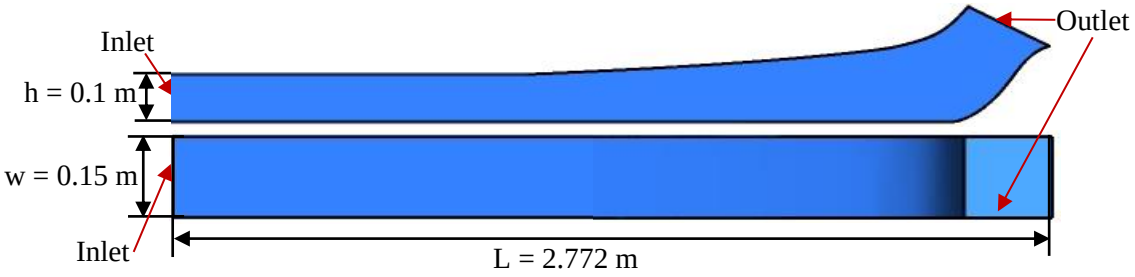

Figure 4. Geometry of the numerical test case, side and top view.

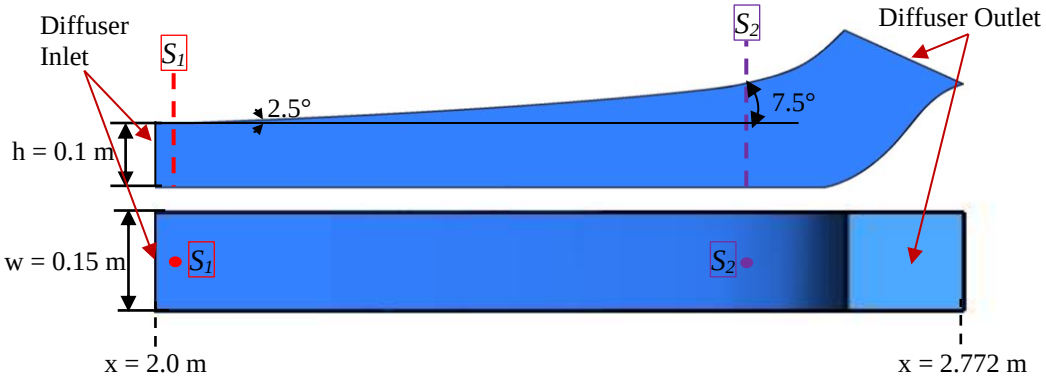

Figure 5. Asymmetric diffuser detail.

The mesh was generated in ICEM CFD. First, the blocking structure also known as 3D bounding box was created. After the blocking topology is created, it can be modified to fit the

geometry properly by splitting the initial block into smaller ones for a further, more detailed blocking topology. The blocking topology was adjusted through various tools, such as splitting or merging the blocks, modifying edges or faces, move vertices and Ogrid definition. The blocking topology created for generating the mesh for the numerical test case is presented in Figure 6 [27].

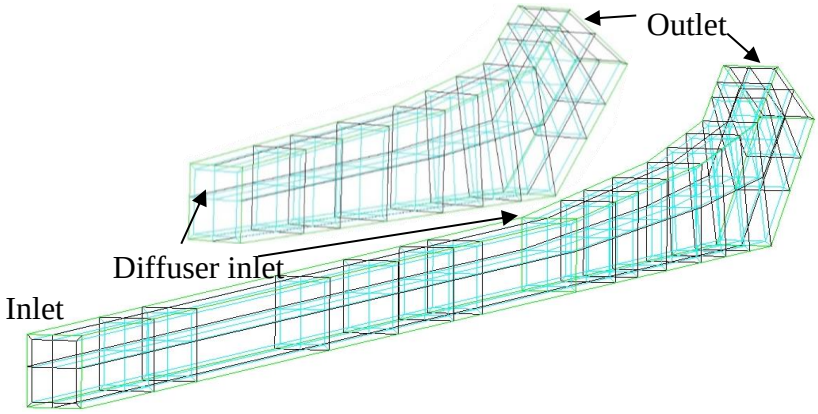

Figure 6. Blocking structure, with zoom for the asymmetric diffuser.

The solver used in the numerical simulations presented in this thesis is Code_Saturne. Code_Saturne can handle both structured and unstructured meshes. Because of the complexity of the geometry of the asymmetric diffuser, an unstructured mesh was created. Therefore, the mesh was initially generated as a structured mesh and then converted into an unstructured mesh. This conversion allows keeping the advantage of the alignment of structured mesh cells and the advantage of the connectivity to the geometry of an unstructured mesh [28]. The generated mesh for the asymmetric diffuser is an unstructured mesh with dominant hexahedral cells, an example of the mesh required for the asymmetric diffuser is presented in Figure 8, Figure 7 and Figure 9.

Figure 7. Mesh domain.

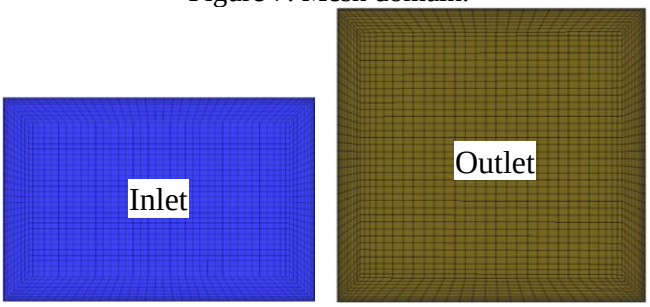

Figure 8. Mesh domain, inlet and outlet view.

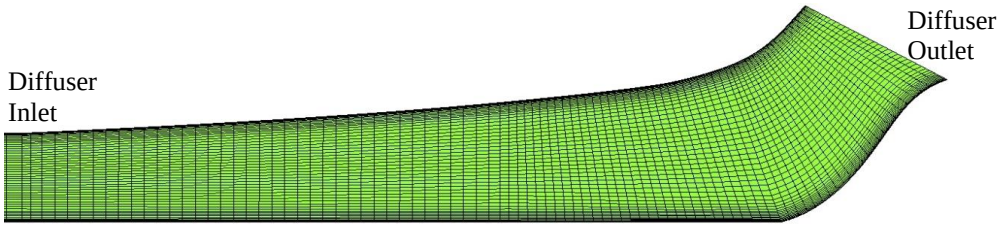

Figure 9. Mesh diffuser detail, cross-section through the centre of geometry view.

The generated mesh must meet the minimum mesh quality conditions imposed by the CFD solver, Code_Saturne. After the simulation setup is completed, the simulation process consists in following three steps: mesh processing, variables computation and output of the numerical solution. Most of the time the mesh quality criteria verified by the CFD solver are not the same as the mesh quality criteria available in the mesh generation software. Therefore, the compatible mesh quality parameters from ICEM CFD that correspond with the required mesh quality parameters from Code_Saturne solver were analysed [27], [28]. The compatible ICEM CFD mesh quality parameters with the Code_Saturne solver mesh quality parameters are: aspect ratio, minimum angle, volume change and warpage.

In Code_Saturne the quality of the mesh is verified at the beginning of the numerical simulation. The cells with unsatisfactory quality are marked as "bad cells", requiring an improvement in the quality of the mesh. The mesh quality criteria verified by Code_Saturne solver are cell's non-orthogonality (Q_f^{ortho}), cell's offset (Q^{offset}), cell's distortion (Q_{LSQ}), cell's volume ratio (Q_{vol}) and the "guilt by association" [28].

The results of the mesh quality analysis are presented at the beginning of each simulation, as the number of bad cells and as in percentage of bad cells for each of the five quality criteria. After reading the meshes in Code_Saturne, the pre-processor returned no errors regarding the mesh quality for all numerical simulations of steady and pulsating flows.

Numerical simulations settings

For the numerical analysis performed for the asymmetric diffuser test case, three simulations using RANS k-ω SST were carried out. The simulations were made using the Code_Saturne CFD solver, using the k-ω SST turbulence model. The settings applied to the numerical simulations are presented further for both steady-state and unsteady-state regimes.

In this thesis the work of Manhart and Duprat was further extended to the following analyses. Firstly, the wall models of Manhart and Duprat were used in less expensive numerical simulations, RANS rather than DNS and LES, and on a more complex geometry than the cases used in the initial analyses conducted by Manhart and Duprat. Secondly, the wall models of Manhart and Duprat were used in carrying out steady and unsteady pulsating flows numerical simulations, not only in steady state LES as presented in Duprat [11]. Thirdly, all the numerical simulations results presented in this thesis were compared with detailed experimental measurements available from Cervantes and Engström [12].

The steady-state numerical simulations were performed using the SIMPLE algorithm for coupling the pressure with velocity, while for the unsteady-state numerical simulations, the SIMPLEC algorithm was used. For computing the gradient of cells for each flow variable, the least-squares method with an extension to the neighbouring cells was used. The Second Order Linear Upwind (SOLU) scheme was used for computing the velocity field and turbulent variables, k and ω [28].

The boundary conditions were set in the same way for all numerical simulations, accordingly to the experimental conditions, except for the inlet boundary condition. The locations of the boundary conditions are presented in Figure 10, and they are color-coded: inlet of the domain is coloured in blue; the walls of the domain are represented with grey, and the

outlet of the domain is marked with green. For the unsteady-state numerical simulations it was used a symmetry plane marked with red colour.

The inlet boundary condition for the steady-state numerical simulations was set to a steady velocity of 0.165 m/s, normal to the surface of the inlet rectangular straight duct. Based on the work of Salehi et al. (2017), the turbulent intensity was set to 3.0 %, which corresponds to a medium turbulent intensity [13].

For unsteady-state numerical simulations, the velocity at the inlet boundary condition was set to a periodic function, equation (21). Three different flow regimes were simulated based on the frequency of the pulsating flows oscillations f_1 = 0.35 Hz, f_2 = 0.10 Hz and f_3 = 0.03 Hz.

$$U = U_0 \cdot \left(1 + \left(A_{Uc} / U_c\right) \cdot \cos\left(2\pi f \cdot t\right)\right) \quad (21)$$

where U_0, (A_{Uc} / U_c), f and t are the mean velocity, the perturbation of the oscillation signal, the frequency of the pulsating flow and the current time.

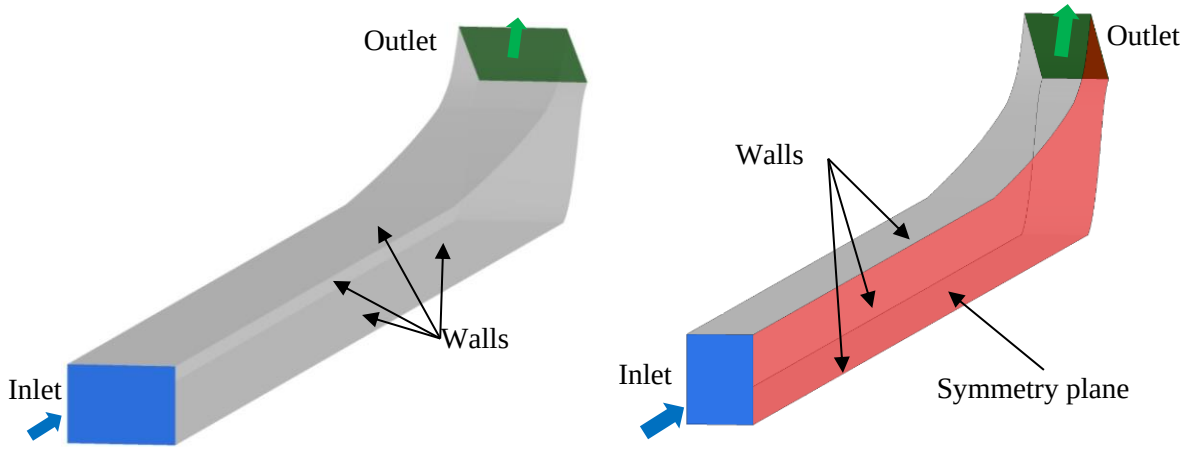

Figure 10. Asymmetric diffuser test case - boundary conditions.

The outlet and the walls were set in the same way for all numerical simulations, steady and unsteady. The flow that exits from the experimental test case is in contact with the atmospheric pressure. Therefore, an outlet boundary condition with an atmospheric pressure of 0 Pa relative pressure was set at the exit of the numerical test case. Since the material for the walls of the experimental test case was Plexiglas, the walls boundary conditions of the numerical test case were set as smooth walls with the “no-slip” condition applied. For reducing the computational effort, for the unsteady-state numerical simulations, it was used a symmetry plane at the half width (z = 0.075 m) of the asymmetric diffuser geometry.

NUMERICAL RESULTS VALIDATION

Experimental data

The experimental data were obtained by Cervantes and Engström [12]. The measurements were carried out in the asymmetric diffuser marked with the red discontinued red line in Figure 3. The experimental data were processed to obtain time-averaged flow variables, time-development flow quantities, phased-averaged flow variables. The experimental flow quantities presented in this section are used with the consent of the authors of the experiment and processed to validate the numerical simulations results performed in this thesis.

- Time-averaged flow variables

The time-averaged flow variables used in the validation of the numerical simulations are the dimensionless streamwise velocity, U^+, (Figure 11) and dimensionless turbulence production, $P_k{}^+$, (Figure 12). The friction velocity, u_τ, used for normalizing U^+ and $P_k{}^+$, was determined using a fifth order polynomial approximation based on equation (22) [12], valid for a $y^+ \leq 12$.

$$U = \frac{u_\tau^2}{\nu} y + \frac{1}{2\rho\nu}\frac{dP}{dx} y^2 + Dy^4 + Ey^5 \qquad (22)$$

where y is the distance from the wall to the computational point, dP/dx is the pressure gradient in the streamwise direction, D and E are free parameters.

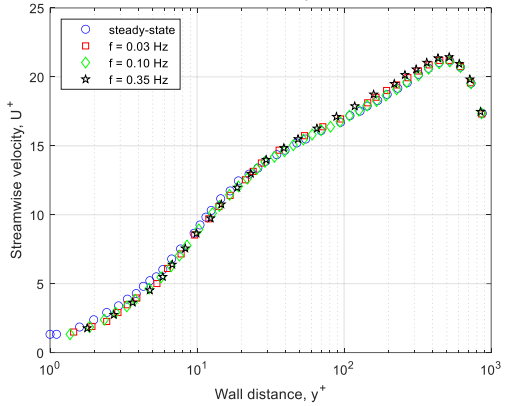

Section S_1

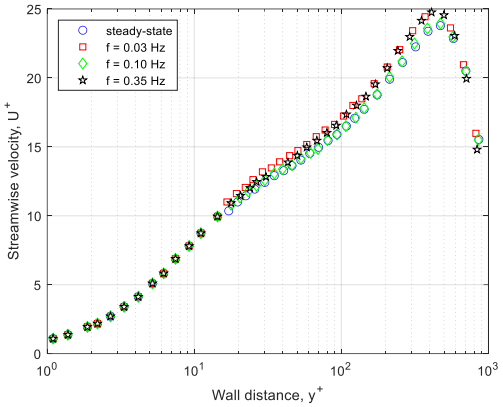

Section S_2

Figure 11. Experimental time averaged streamwise velocity, U^+

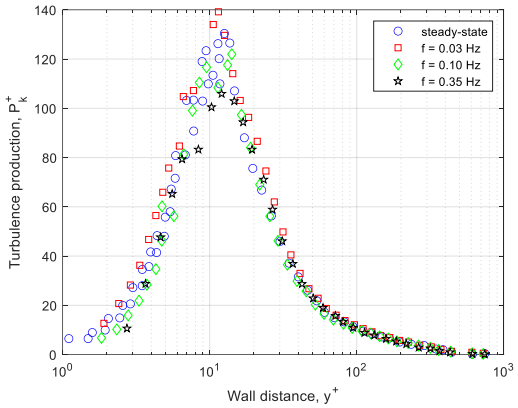

Section S_1

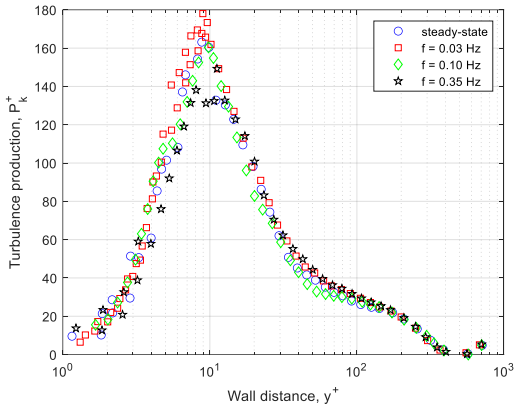

Section S_2

Figure 12. Experimental time averaged turbulent production, $P_k{}^+$

- Time-development flow quantities

The time-development flow variables used in the comparisons of the numerical simulations and experimental data are the centreline velocity, U_p, (Figure 13) and wall shear stress, τ_w, (Figure 14). The velocity measured in the centreline of the diffuser, U_p, was normalized with its mean value, U_c. The development in time of the centreline velocity was reduced to one period as the flows are periodic. The variation in time of the normalized wall shear stress with its mean value, τ_m. is presented for one period, in Figure 14.

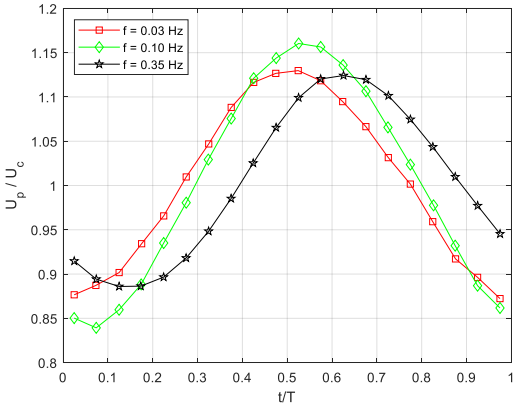

Section S_1

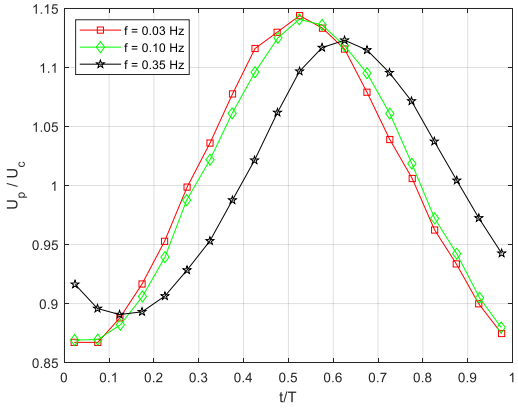

Section S_2

Figure 13. Experimental time development of centreline velocity normalized with mean centreline velocity, U_p / U_c

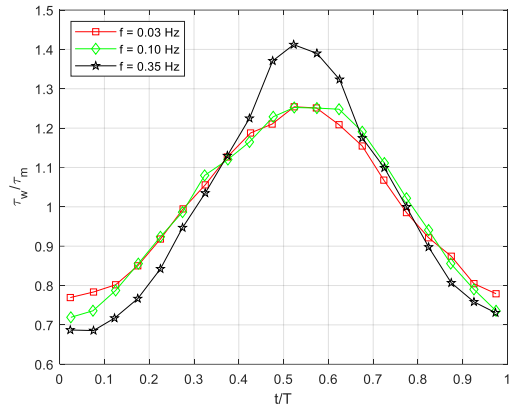

Section S_1

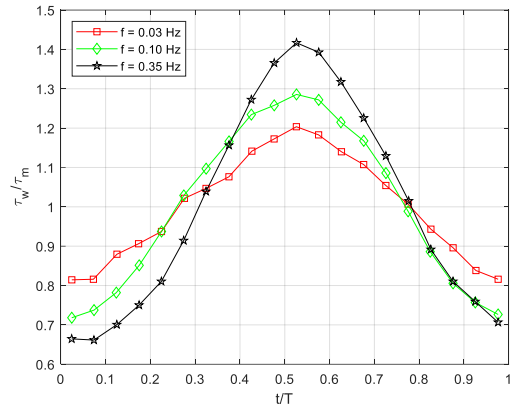

Section S_2

Figure 14. Experimental time development of wall shear stress normalized with the mean wall shear stress, τ_w / τ_m

- Phased-averaged flow variables

The phased-averaged flow variables used in the validation of the numerical simulations are the amplitude of streamwise oscillating velocity, A_U, (Figure 15) and phase shift of the streamwise oscillations, φ_U, (Figure 16).

The amplitude of streamwise oscillating velocity, A_U, from experiment was normalized with its value at the centre of the asymmetric diffuser, A_{Uc}, and is presented in Figure 15. The difference between the experimental phase of the streamwise velocity oscillation, ϕ_U, and its centre value, ϕ_{Uc}, is presented in Figure 16. The continuous line represents the amplitude of the Stokes solution in a channel.

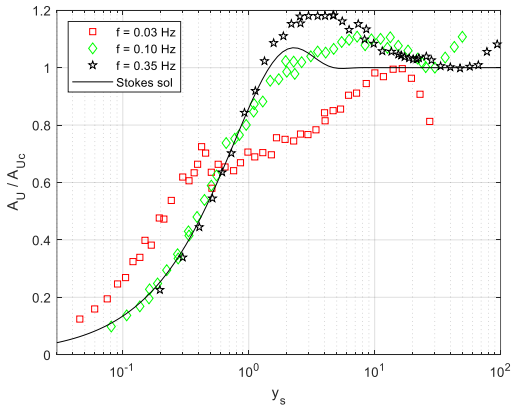

Section S_1

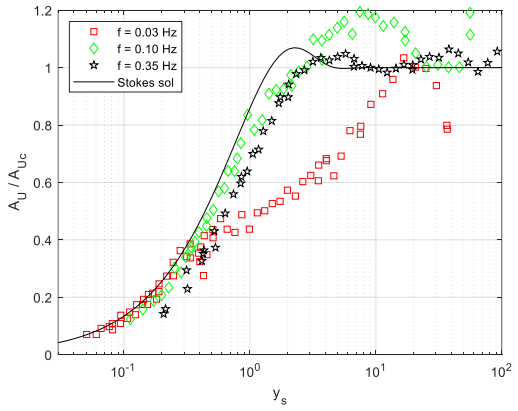

Section S_2

Figure 15. Experimental amplitude of the streamwise oscillating velocity normalized with the centre streamwise amplitude, A_U / A_{Uc}

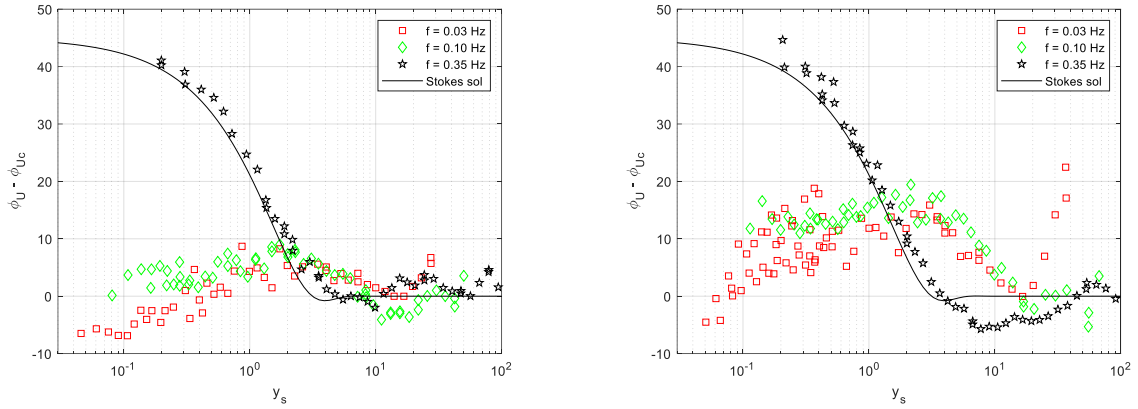

Section S_1 Section S_2

Figure 16. Experimental phase shift of the streamwise oscillation relative to the centre streamwise velocity, ϕ_U / ϕ_{Uc}.

The experimental data are used to validate the numerical simulations results carried out using the three wall models (*k-ω* SST, Manhart *k-ω* SST and Duprat *k-ω* SST), for one steady flow and three pulsating flows with the frequencies of 0.35 Hz, 0.10 Hz and 0.03 Hz.

Steady flow numerical simulations results

The validation of the steady flow numerical simulation results with the experimental data is performed for the time-averaged variables: streamwise velocity, U, and turbulent production, P_k. Because the research conducted for this thesis is focused on the boundary layer, all the numerical simulations carried out are based on the *k-ω* SST turbulence model. The experimental data used in the validation of the numerical simulations was available from the work of Cervantes and Engström [12]. Furthermore, the numerical results were compared against detailed numerical simulations of Reynolds Stress Model (RSM) [29] performed by Salehi et al. [13]. The RSM numerical simulations performed by Salehi et al. [13] are carried out using boundary conditions very similar to the experimental procedure performed by Cervantes and Engström [12]. The comparison of the numerical results with the experimental data was made in two sections from the numeric case: at x = 2.082 m, S_1, and at x = 2.632 m, S_2, the same as the measurement sections (Figure 3).

To determine the right mesh dimension for the steady-state numerical simulations mesh sensitivity studies were performed. The parameters used for the mesh sensitivity studies were the streamwise velocity, U, and the friction velocity, u_τ. To keep a good accuracy of the numerical simulations results and to avoid large computational costs, from the comparisons performed in the mesh sensitivity study resulted that the normal size mesh can be chosen for the validation of the numerical simulations. Table 2 presents the mesh quality parameters for the normal size mesh used to carry out the numerical simulations for all wall models.

Table 2 Meshes used for numerical simulations

Numerical simulation	Mesh size	Mesh quality parameters			
		Angle (min.) [°]	Aspect ratio (max.) [-]	Volume change (max.) [-]	Warpage (max.) [°]
k-ω SST	$1.018 \cdot 10^6$	40.59	127	2.75	5.39
Manhart k-ω SST / *Duprat k-ω* SST	$0.528 \cdot 10^6$	41.22	46.1	2.42	5.39

The numerical simulations results are carried out for each wall model using the appropriate mesh requirements: for the standard *k-ω* SST wall model is used a mesh of 1018487

cells where the average y^+ is 0.4, and for the Manhart and Duprat wall models is used a mesh of 528853 cells where the average y^+ is 1.54 and 1.53 respectively.

Table 3 presents the comparison of the wall shear stress, τ_w, and the friction velocity, u_τ, between the numerical simulations results carried out with the three wall models and the experimental data. All three wall models underestimate the wall shear stress, τ_w, and the friction velocity, u_τ. A cause of the underestimation of the averaged flow quantities, τ_w and u_τ, is the setup of the inlet boundary condition of the numerical case different than in the experimental procedure. Even though the Manhart and Duprat wall models underestimate the averaged flow quantities is worth noted that the results are obtained using half of the mesh size comparing to the standard k-ω SST wall model.

Table 3 Mean flow quantities – steady flows

Test case conditions	Wall shear stress, τ_w [Pa]		Friction velocity, u_τ [m/s]	
	Section S_1	Section S_2	Section S_1	Section S_2
Experimental data	0.090	0.050	0.0095	0.0070
k-ω SST	0.070	0.033	0.0083	0.0057
Manhart k-ω SST	0.064	0.029	0.0080	0.0054
Duprat k-ω SST	0.064	0.029	0.0080	0.0054

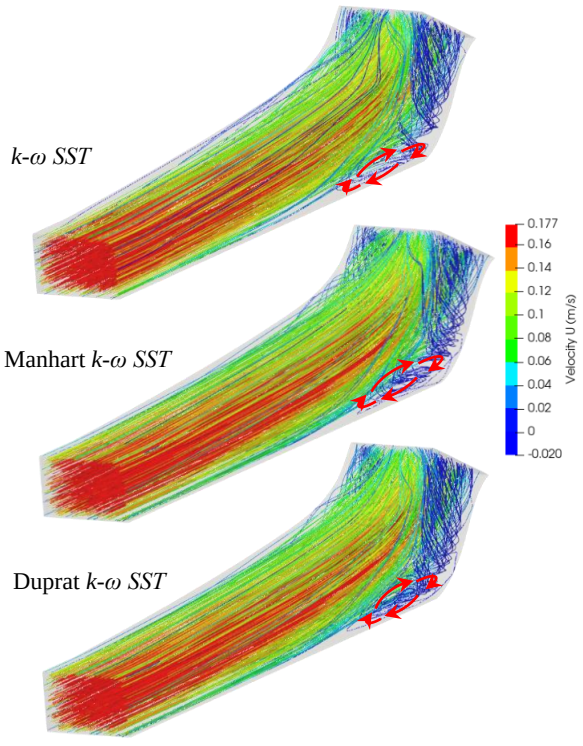

Figure 17. Streamwise velocity streamlines.

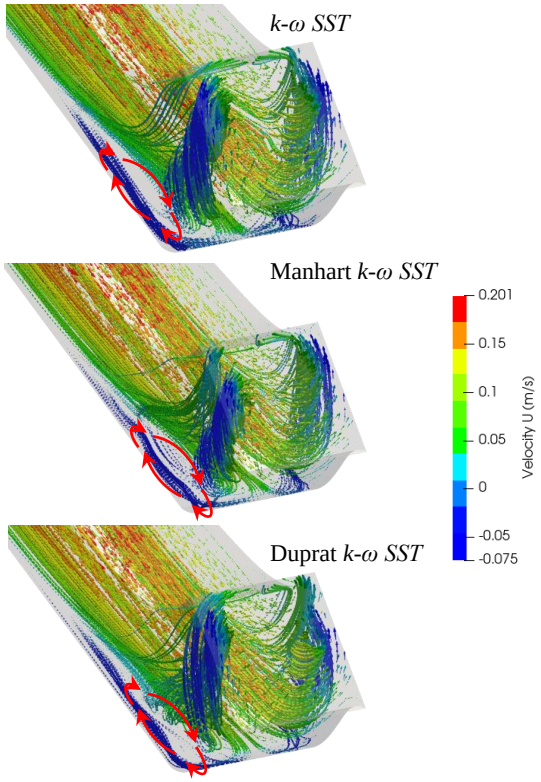

Figure 18. Streamwise velocity vectors.

After the section S_2 a flow recirculation zone, marked with red arrows, is observed in Figure 17 and Figure 18 on each side wall near the curvature of the asymmetric diffuser. Going upward to the diffuser outlet two vortices are formed one on each side of the asymmetric diffuser. The flow recirculation zones show that the flow is influenced by an adverse pressure gradient, also observed in the experimental procedure [12].

- Streamwise velocity profiles, U^+

The distribution of the streamwise velocity, U^+, is presented in Figure 19 for both sections. In section S_1, just before the beginning of the diffuser, the flow is influenced by a favourable pressure gradient which can result that the boundary layer is in equilibrium. Thus,

the experimental mean streamwise velocity in wall units, U^+, follows the general velocity distributions laws of the boundary layer: the linear law in the viscous sublayer ($y^+ \leq 5$) equation (23), and in the logarithmic layer the log-law ($\kappa = 0.41$, $C = 5.2$) equation (24). The results of the numerical simulations show a very good approximation of the mean streamwise velocity, U^+, in the near wall region, viscous and parts of the buffer layers, up to a $y^+ \approx 12$.

$$U^+ = y^+ \tag{23}$$

$$U^+ = \frac{1}{\kappa}\ln y^+ + C \tag{24}$$

To observe the influence of the adverse pressure gradient over the flow field, the second section, S_2, was chosen close to the elbow of the diffuser. The influence of the adverse pressure gradient due to the diverging top wall of the diffuser can be seen comparing the standard log-law with the experimental data. Starting with the buffer layer and continuing in the logarithmic layer the results of the numerical simulations carried with the three wall models fail to estimate the experimental data. Although, the Manhart and Duprat wall models are developed to yield good results in flows influenced by the adverse pressure gradient, the complexity of the asymmetric diffuser geometry is creating difficulties in estimating the experimental data.

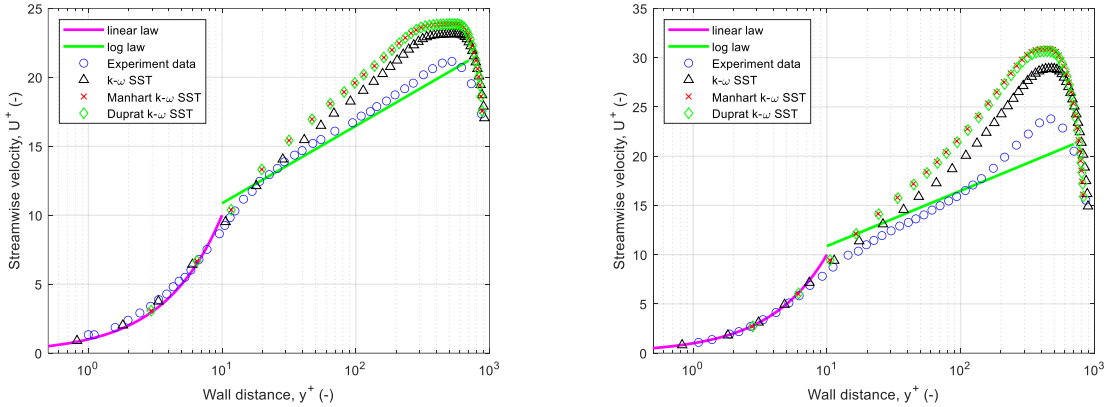

Section S_1 Section S_2

Figure 19. Mean streamwise velocity distribution, U^+ vs y^+.

It is important to note that the accuracy of the Manhart and Duprat wall models, which is close to the standard *k-ω* SST wall model is achieved using half of the mesh required by the standard *k-ω* SST wall model. Also, the computation time to perform a numerical simulation is smaller for the Manhart and Duprat wall models than for the *k-ω* SST wall model. The computation time required to perform the numerical simulations carried out using the three wall models is presented in Table 4.

Table 4 Wall models performance – steady flows

Numerical simulation	Mesh size	Average y^+	Computation time
***k-ω* SST**	$1.018 \cdot 10^6$	0.4	3h 26’
Manhart *k-ω* SST	$0.528 \cdot 10^6$	1.54	3h 19’
Duprat *k-ω* SST		1.53	3h 10’

- Turbulent production, P_k^+

The averaged turbulent production, P_k^+ for the numerical simulations performed with the three wall models is presented in Figure 20. The results from the three numerical simulations follow the trend of the experimental data for both considered sections, S_1 and S_2. Still, all wall models poorly estimate the level of the averaged turbulent production, especially in the first part of the boundary layer, viscous and buffer layers, up to a $y^+ \approx 40$ for section S_1 and up to a

$y^+ \approx 20$ for section S_2. The underestimation of the production of the turbulent kinetic energy of the numerical simulations results for all wall models may come from the evaluation of the poor estimation of the wall shear stress.

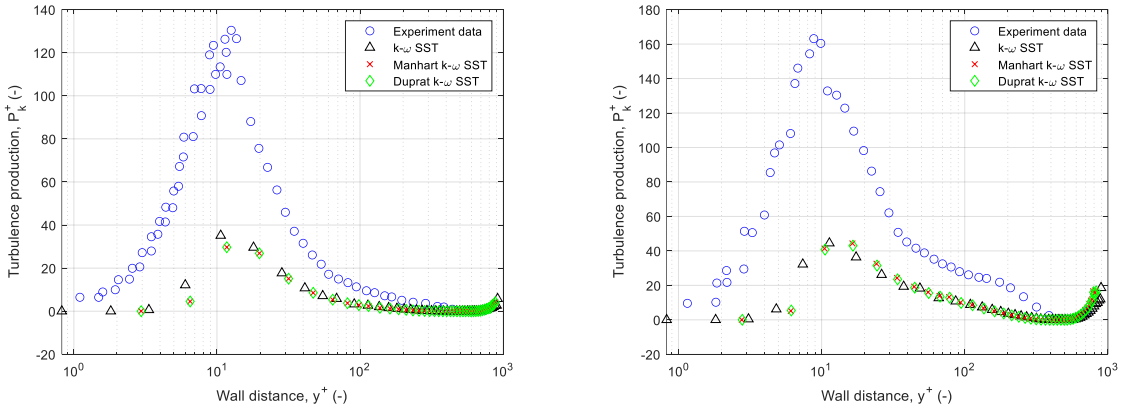

Section S_1 Section S_2

Figure 20. Averaged turbulent kinetic energy production, P_k^+ vs y^+.

Pulsating flows numerical simulations results

The validation of the pulsating flows numerical simulation results with the experimental data is carried out for time-averaged flow variables, time-development flow variables and phased-averaged flow variables. The unsteadiness of the pulsating flows is based on three frequencies: f_1 = 0.35 Hz, f_2 = 0.10 Hz, f_3 = 0.03 Hz.

For the unsteady-state numerical simulations, sensitivity studies were performed. These studies were divided into several parts: mesh sensitivity study, time step sensitivity study, and a periodic sensitivity study due to the numerical simulation's periodic behaviour. First, the mesh sensitivity analysis is carried out to find the right balance between the computational effort and spatial discretization error. Second, the time-step sensitivity analysis is conducted to find the right time-step that will respect the Courant–Friedrichs–Lewy (CFL) condition and will adequately simulate the behaviour of the pulsating turbulent flows. Third, due to the repetitive nature of the pulsating flow oscillations, the periodic state of the pulsating flows is studied.

To generate the appropriate mesh distribution and set the correct settings of the numerical simulations for the 3D asymmetric diffuser test case, the Stokes second problem was used for all three pulsating flows frequencies: 0.35 Hz, 0.10 Hz, and 0.03 Hz.

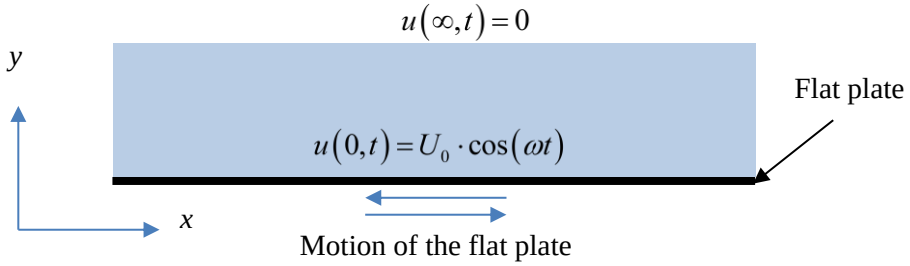

Figure 21. Stokes second problem description.

The exact solution of the Stokes second problem for an oscillating flat plate in a laminar flow, equation (25), was selected as the reference for the sensitivity studies.

$$u(y,t)=U_0\cdot e^{-y/l_s}\cdot\cos(\omega\cdot t-y/l_s) \quad (25)$$

where U_0 is the velocity magnitude, t is the time, ω is the angular frequency, y is the coordinate normal to the boundary, l_s is the Stokes length.

Analysing the comparisons from the sensitivity studies, resulted that in the numerical simulations performed for the asymmetric diffuser, several important criteria were considered:

- The mesh distribution normal to the wall should consist in at least 50 cell layers, uniform in height, throughout the entire height of the oscillating layer, while considering the boundary layer requirement, y^+.
- To accurately represent the oscillations of the pulsating flow, the time-step of the numerical simulations should be considered to result in at least 40 data points over one period of the oscillations.
- It is important to determine the time-step that will respect the CFL condition when performing unsteady-state numerical simulations, therefore the maximum Courant number should not exceed 50.

- Asymmetric diffuser meshes

Based on the mesh sensitivity study the meshes used for the pulsating flows numerical simulations of the asymmetric diffuser were generated for each wall model of each frequency, Table 5.

From the previous subchapters results that to perform a pulsating flow numerical simulation a very fine mesh discretization in the near-wall region is required to accurately evaluate the velocity distribution in the oscillating boundary layer. Thus, the meshes generated for the unsteady-state numerical simulations would easily reach the order of millions of cells. To reduce the computational effort of carrying out unsteady-state numerical simulations of pulsating flows the meshes were generated for half of the geometry, by halving the width (z = 0.075 m) of the channel, presented in Figure 22.

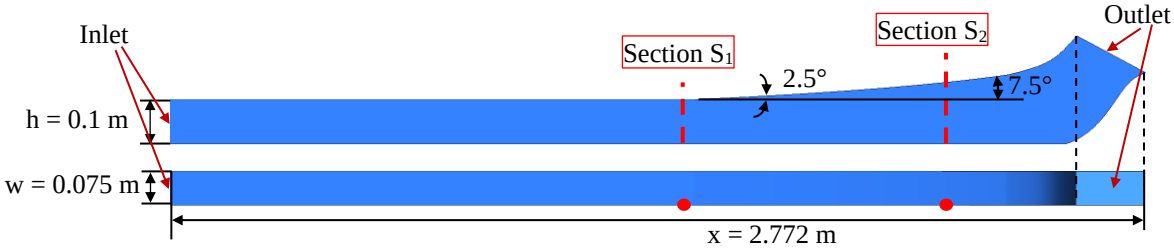

Figure 22. Half width geometry (z = 0.075 m).

Table 5 Meshes used for the unsteady numerical simulations

Frequency	***f_1* = 0.35 Hz**	***f_2* = 0.10 Hz**		***f_3* = 0.03 Hz**	
Wall model	*k-ω* SST *Manhart k-ω* SST *Duprat k-ω* SST	*k-ω* SST	*Manhart k-ω* SST *Duprat k-ω* SST	*k-ω* SST	*Manhart k-ω* SST *Duprat k-ω* SST
Mesh size (cells)	$4.467 \cdot 10^6$	$7.195 \cdot 10^6$	$4.591 \cdot 10^6$	$11.800 \cdot 10^6$	$5.317 \cdot 10^6$

Based on the time-step sensitivity analysis of the Stokes second problem test case, for the unsteady-state numerical simulations, the time-step of Δt = 0.01 s needs to be imposed to respect the CFL condition for all three frequencies regardless of the wall model used. Still, as observed in the Stokes 2nd problem test case, a time-step of 0.01 s, considering the refinement of the mesh discretization for each wall model and frequency, will lead to large amounts of computational storage. Therefore, two time-steps were used for the unsteady-state numerical simulations of the pulsating flows:

- one time-step used for the computation of the flow variables, Δt_c = 0.01 s,
- another time-step used for sampling the data from the numerical simulations, Δt_s, that will result in 48 sampling data points over one period of the pulsating flows.

The Courant number used in carrying out the numerical simulations for each pulsating flow frequency of 0.35 Hz, 0.10 Hz and 0.03 Hz are presented in Table 6.

Table 6 CFL condition, maximum Courant number

Wall model	Frequency (Hz)		
	0.35	0.10	0.03
k-ω SST	3.85	3.94	28.41
Manhart *k-ω* SST	4.03	4.85	4.61
Duprat *k-ω* SST	21.23	16.3	4.61

The state of periodicity of the pulsating flows numerical simulations was studied using monitor points located at the beginning of the asymmetric diffuser (section S_1) at different distances from the bottom wall of the diffuser. The monitor points are located on the symmetry plane (z = 0.075 m) at different distances from the wall: 0.001 m, 0.01 m, 0.02 m and 0.05 m.

The periodic convergence of the numerical simulations was performed for the streamwise velocity, U, over the simulation time for each numerical simulation. For the 0.35 Hz frequency all three wall models reached the periodic convergence after the 7th period. For the 0.10 Hz frequency only the *k-ω* SST wall model and the Manhart *k-ω* SST wall model attained the periodic convergence at the 3rd period of the simulation. The Duprat *k-ω* SST wall model failed to reach the periodic convergence and after the 6th period Code_Saturne solver stopped due to divergence in the computation. The periodic convergence for the frequency of 0.03 Hz was obtained from the 2nd period for all three wall models.

The numerical simulations of the pulsating flows were carried out using the same wall models used for the steady-state numerical simulations: the *k-ω* SST, the Manhart *k-ω* SST, and the Duprat *k-ω* SST. The comparison was carried out at the same sections used for the comparison of the steady-state numerical simulations, at section S_1 and section S_2.

The quantities presented in the following comparisons were reduced to one period, after the periodic state was reached. Depending on the pulsating flow oscillation frequency several periods are required to reach the periodic state of the numerical simulations:

- for the frequency of f_1 = 0.35 Hz, seven periods were required to attain the periodic state, and the results of the numerical simulations were extracted from the 8th period, between 21.06 and 23.94 seconds.
- for the frequency of f_2 = 0.10 Hz, three periods were required to reach the periodic state, and the extraction of the of the numerical simulations results was performed at the 4th period, from 34.65 to 44.73 seconds.
- for the frequency of f_3 = 0.03 Hz, two periods were required to achieve the periodic state, and the numerical simulations results were extracted at the 3rd period, from 82.6 to 116.2 seconds.

The validation of numerical simulations was performed for three groups of flows quantities structured as follows: time-averaged quantities, time-development quantities and phased-averaged quantities.

The simulation running time can have a major impact when conducting a numerical analysis. Therefore, the time elapsed for each numerical simulation used in the validation procedure for the pulsating flows numerical analysis is presented in Table 7.

Due to the instabilities generated by the Duprat wall model in the Code_Saturne solver for 0.35 Hz and 0.10 Hz frequencies, the time required to reach the simulation time was higher than for the *k-ω* SST or Manhart *k-ω* SST numerical simulations. It is important to consider that the Duprat wall model was not used until this thesis, to the knowledge of the author of the thesis, in any other numerical simulations than for steady flows. For a lower frequency, 0.03 Hz, that is closer to a steady flow than the other two frequencies, the Duprat wall model returns the fastest results.

Table 7 Simulations running time – pulsating flows

Wall model	Frequency 0.35 Hz Simulation time 25.74 s	Frequency 0.10 Hz Simulation time 51 s	Frequency 0.03 Hz Simulation time 133 s
k-ω SST	36.7 hours	159.3 hours	599.8 hours
Manhart *k-ω* SST	35.1 hours	69.4 hours	127.2 hours
Duprat *k-ω* SST	298.1 hours	429.8 hours	115.5 hours

- **Time-averaged flow variables**

Time-averaged flow variables used in the validation of the pulsating flows numerical simulations are the wall shear stress, τ_w, the friction velocity, u_τ, the dimensionless streamwise velocity, U^+, and the dimensionless turbulence production, P_k^+.

The wall shear stress, τ_w, and the friction velocity, u_τ, resulted from the numerical simulations of each wall model are compared with their corresponding experimental data for both sections of each frequency and presented in Table 8.

Table 8 Mean flow quantities – pulsating flows

Test case	Wall shear stress, τ_w (Pa)		Friction velocity, u_τ (m/s)	
	Section S_1	*Section S_2*	*Section S_1*	*Section S_2*
Frequency 0.35 Hz				
Experimental data	0.087	0.046	0.0093	0.0068
k-ω SST	0.067	0.032	0.0081	0.0056
Manhart *k-ω* SST	0.067	0.033	0.0081	0.0057
Duprat *k-ω* SST	0.067	0.033	0.0081	0.0057
Frequency 0.10 Hz				
Experimental data	0.09	0.049	0.0095	0.0070
k-ω SST	0.067	0.032	0.0081	0.0057
Manhart *k-ω* SST	0.065	0.031	0.0081	0.0055
Duprat *k-ω* SST	0.063	0.029	0.0079	0.0054
Frequency 0.03 Hz				
Experimental data	0.09	0.045	0.0095	0.0067
k-ω SST	0.067	0.033	0.0082	0.0057
Manhart *k-ω* SST	0.064	0.030	0.0080	0.0055
Duprat *k-ω* SST	0.064	0.030	0.0080	0.0055

The values of the wall shear stress and the friction velocity are reduced to one period after the convergence periodicity was attained. Comparing the experimental data with the results of the numerical simulations it can be observed that the wall models underestimate the wall shear stress and the friction velocity in each section for all considered frequencies. A possible cause to the discrepancy between the experimental data and the numerical simulation results is represented by the inlet boundary condition.

- Streamwise velocity, *U*

In section S_2 the flow is separating from the walls in the corners of the diffuser where a positive pressure gradient affects the flow. Also in the second section, in the corners of the diffuser, the velocity is negative meaning that regions of flow recirculation occur as observed in Figure 23, which lead to forming of vortices shown in Figure 24.

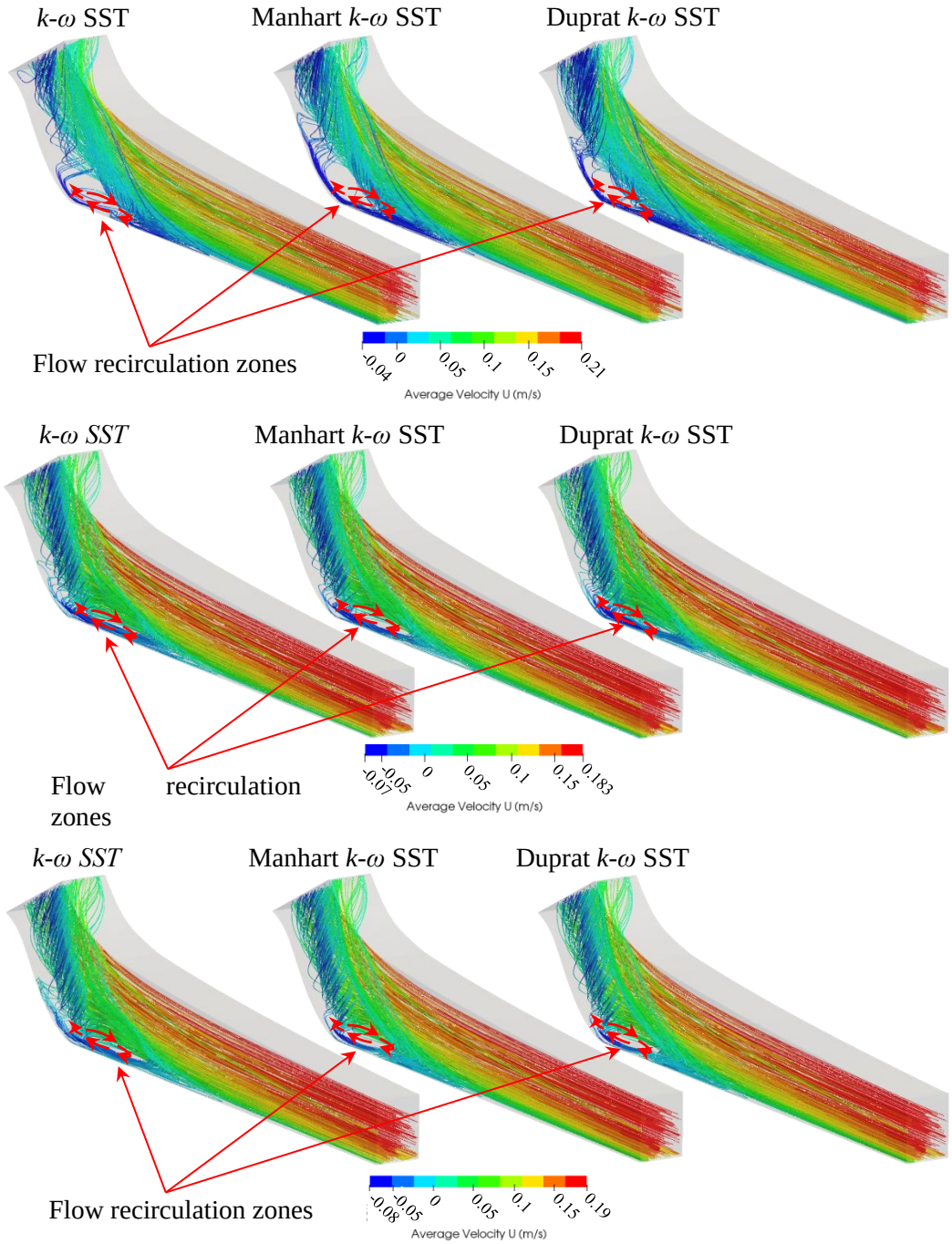

Figure 23. Streamlines of U velocity. From top to bottom the frequencies are 0.35 Hz, 0.10 Hz and 0.03Hz.

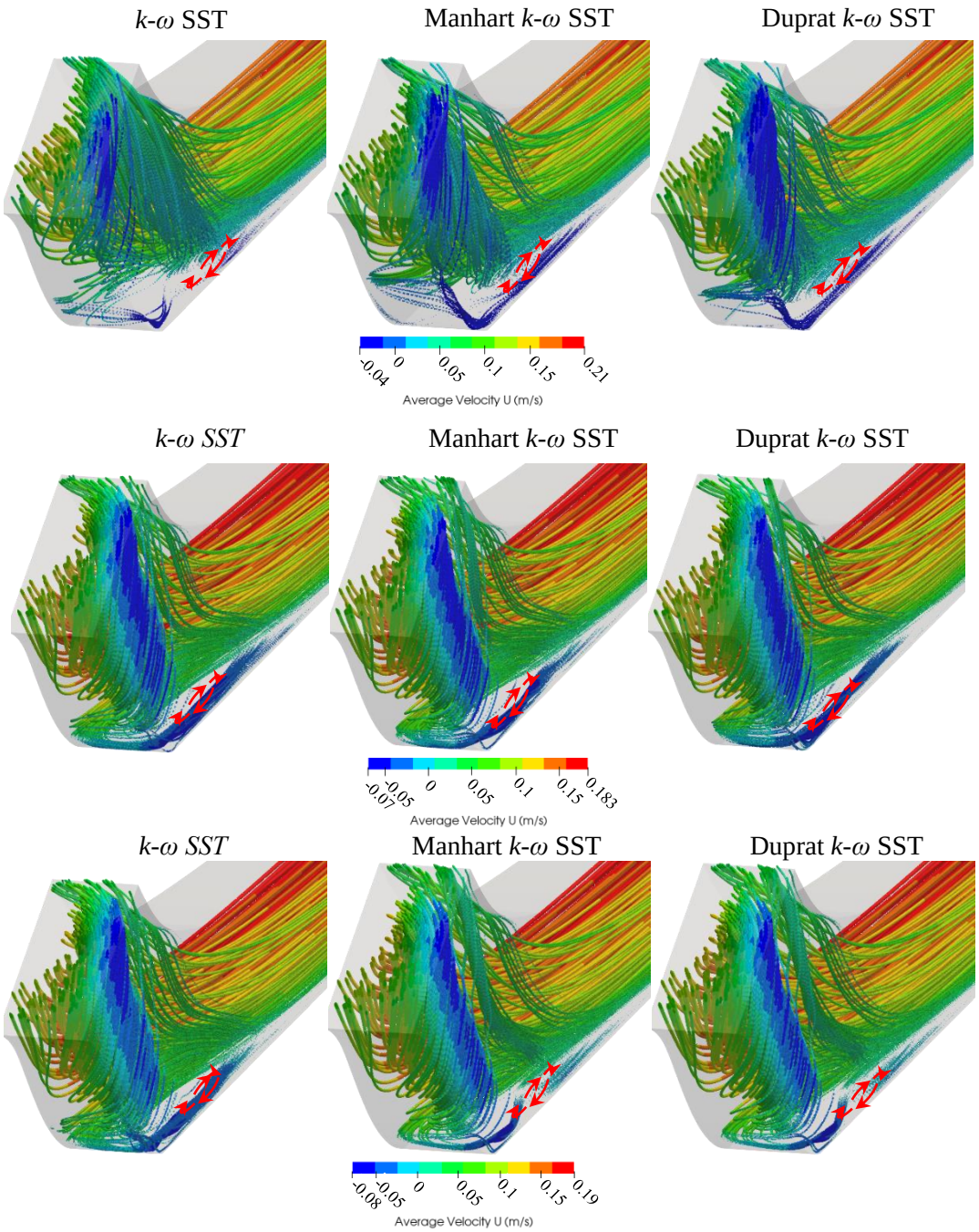

Figure 24. *U* velocity vectors. From top to bottom the frequencies are 0.35 Hz, 0.10 Hz and 0.03Hz.

- Streamwise velocity profiles, U^+

The streamwise velocity distributions of U^+ for the pulsating numerical simulations are presented in Figure 25 compared with the experimental data for each frequency.

The results of the numerical simulations compared to the experimental data shows a good agreement between the data, at least in the near wall region until the distributions reach $y^+ = 10$. After that all three wall models start to fail approximating the experimental data. For the frequency of 0.10 Hz, the Duprat *k-ω* SST shows the most increased deviation in estimating the experimental data because of the instabilities induced in the Code_Saturne solver, leading to a poor periodic convergence of the numerical simulation. For the other two frequencies of 0.35 Hz and 0.03 Hz, the Manhart *k-ω* SST and Duprat *k-ω* SST return the same results.

Although the Manhart and Duprat wall models are in a small percentage less accurate compared to the *k-ω* SST wall model, except for the 0.35 Hz frequency where all wall model's results are almost the same, the Manhart and Duprat wall models use a two times coarser mesh

than the *k-ω* SST wall model. The advantage of using a coarser mesh has a tremendous impact over the time required to perform a pulsating flow numerical simulation and the time economy could reach up to four times compared to the traditional wall models, i.e., *k-ω* SST (Table 7).

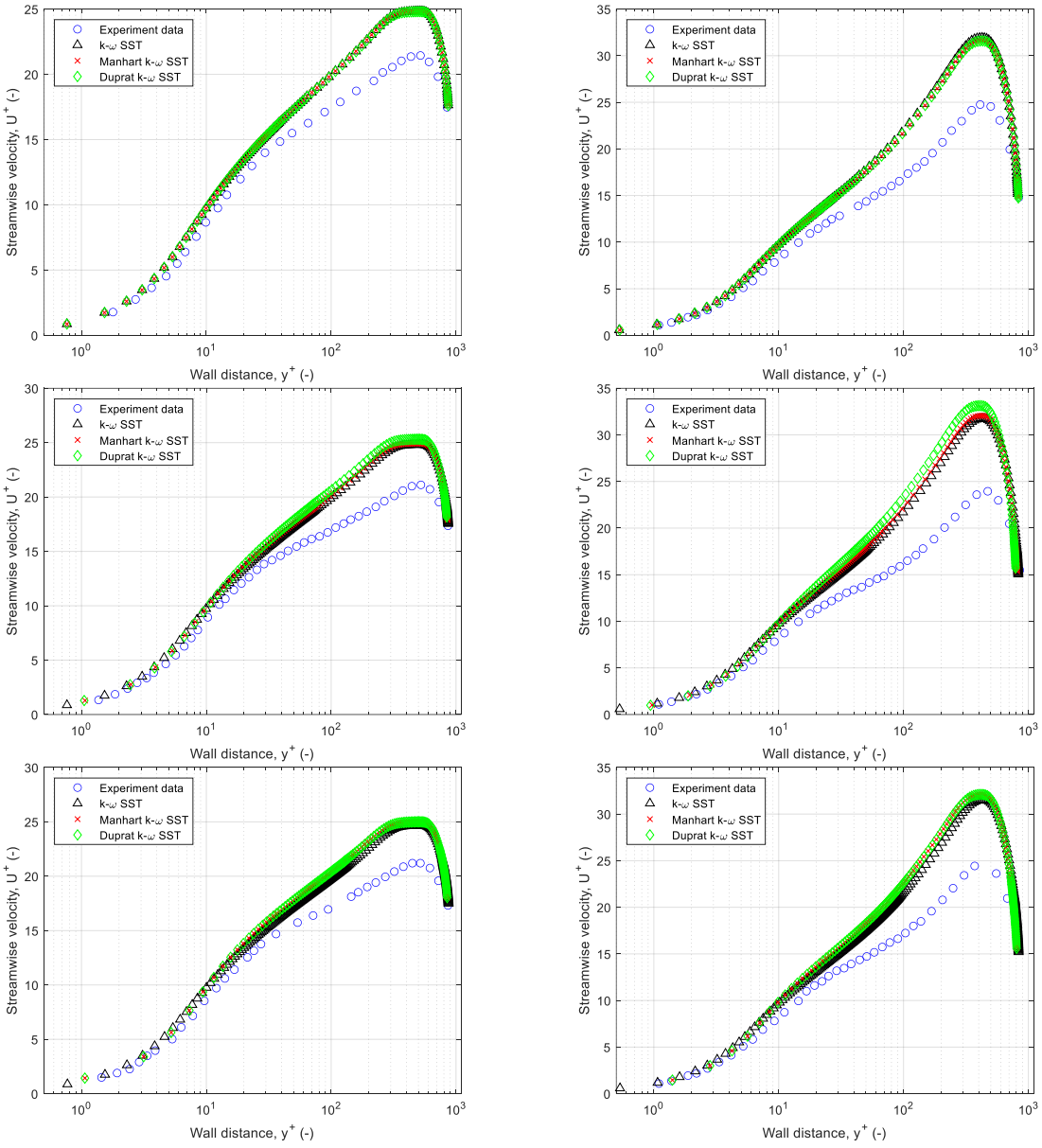

Section S_1 Section S_2

Figure 25. Time-averaged streamwise velocity distribution, U^+ vs y^+. From top to bottom the frequencies are 0.35 Hz, 0.10 Hz and 0.03Hz.

- Turbulent production, P_k^+

The turbulent production distribution, P_k^+, is presented in Figure 26 for all three frequencies in both diffuser sections. In all pulsating flow numerical simulations, the turbulent production, P_k^+, is highly undervalued by all three wall models with approximately 50 % compared to the experimental data, regardless of the considered section, S_1 and S_2. Although the wall models fail to estimate the experimental data, the locations on the *x*-axis of the maximum turbulent production value are predicted very close to the measurement data, for section S_1 at approximately $y^+ = 10$ and for section S_2 at $y^+ = 9$. These comparisons show the disadvantage of the RANS numerical simulations where the eddy viscosity is not estimated correctly due to its definition based on the turbulent kinetic energy, *k*.

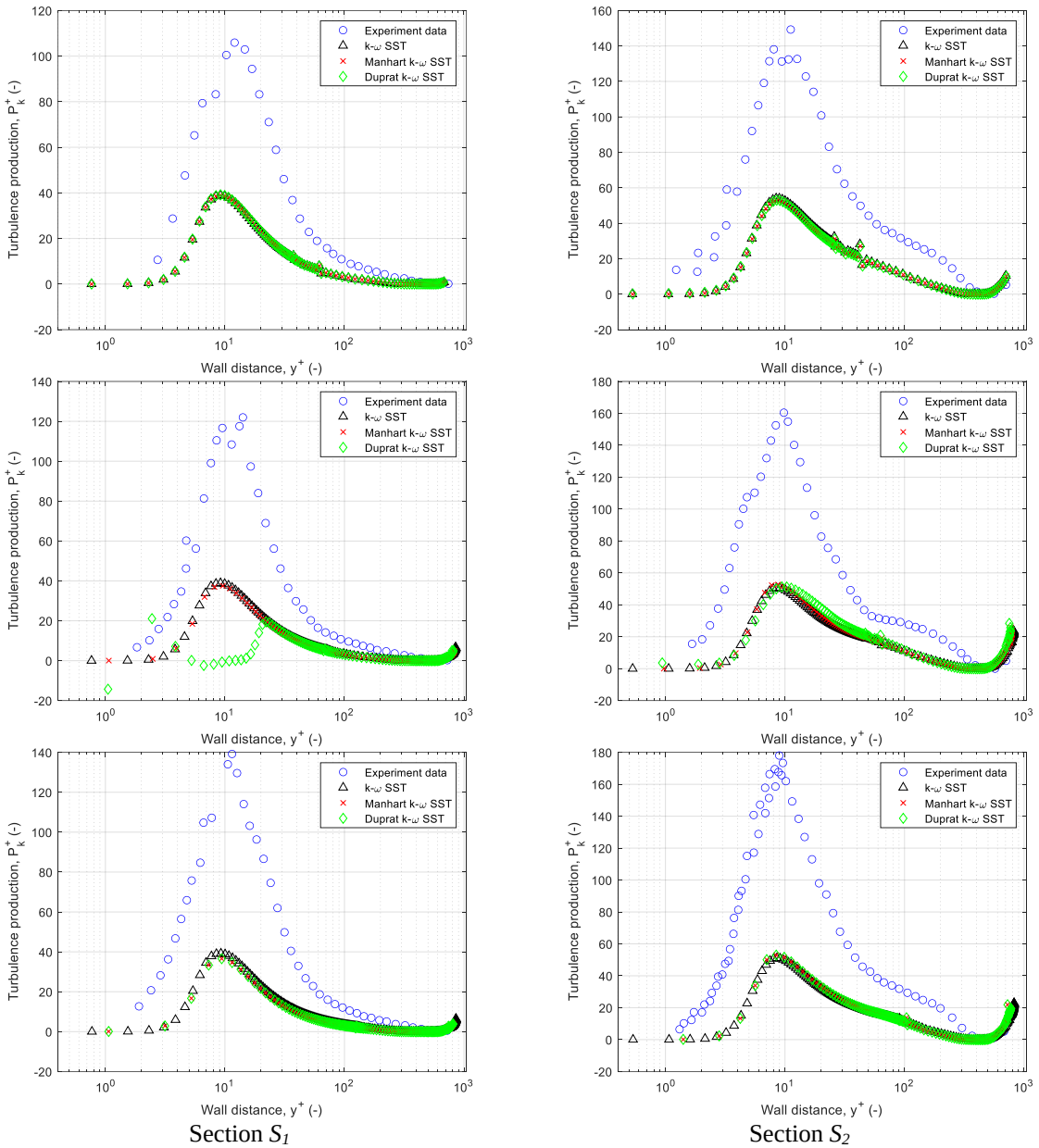

Section S_1 Section S_2

Figure 26. Time-averaged turbulent kinetic energy production, P_k^+ vs y^+. From top to bottom the frequencies are 0.35 Hz, 0.10 Hz and 0.03Hz.

- **<u>Time-development flow variables</u>**

The studied flow variables are the velocity extracted from the centre of the asymmetric diffuser, U_p, and the wall shear stress, τ_w. The flow variables presented in this section are developed in time over one period after the numerical simulation reach its convergence state.

- <u>Centreline velocity, Up</u>

The velocities extracted at the centreline of the asymmetric diffuser, U_p, normalised with the mean velocity, U_c, are presented in Figure 27.

The numerical simulations results are in good agreement with the experimental measurements for the section S_1, for all the data points in the period. For the section S_2, the amplitude of the velocity wave form is underestimated by all wall models. Due to the location of the studied velocity, i.e., in the centre of the diffuser, the results of the numerical simulations are very similar to each other regardless of the mesh used. One source of the differences between the numerical simulations results and the experimental data in section S_2 is the influence of the adverse pressure gradient over the flow in the diffuser.

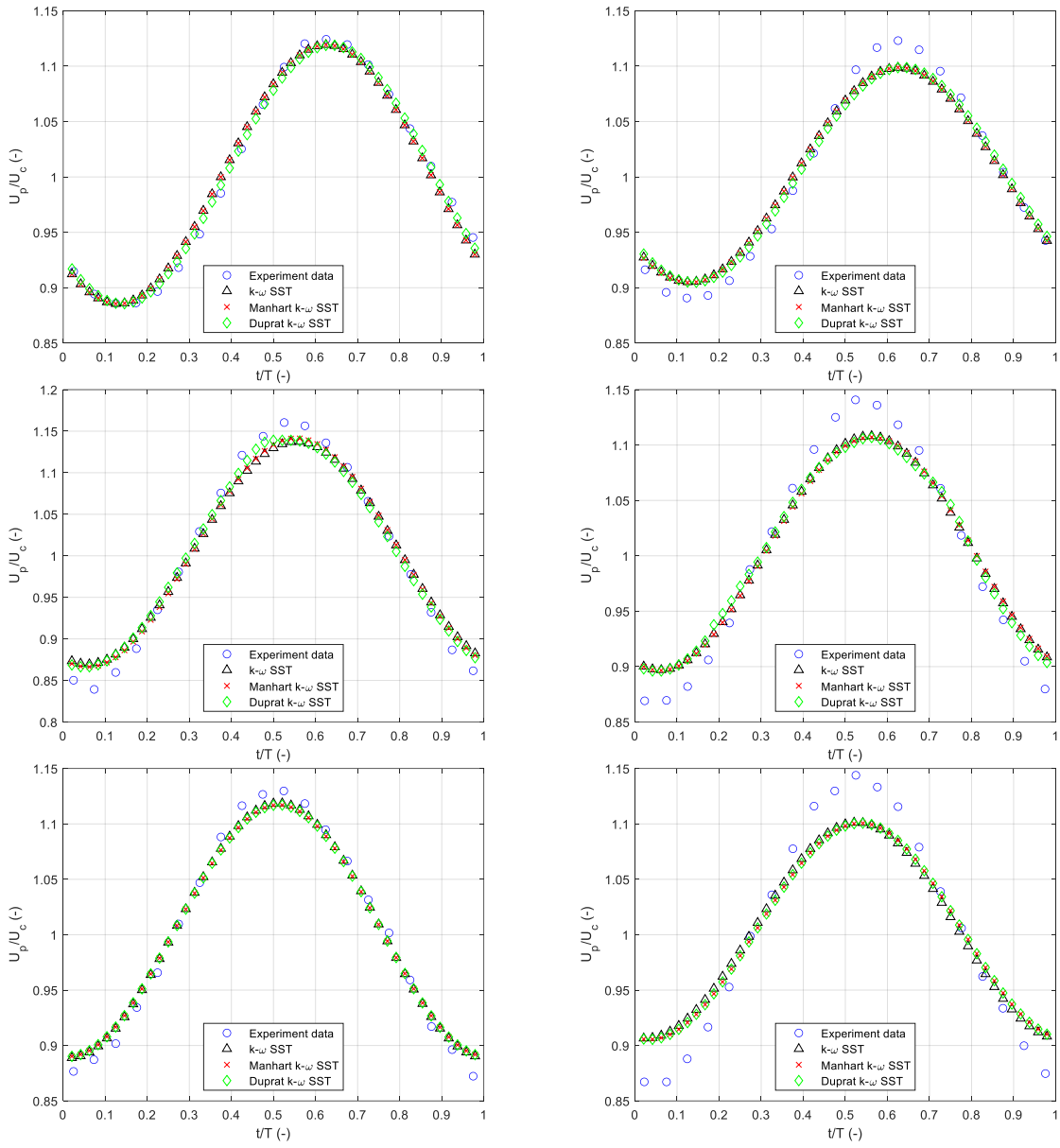

Section S_1 Section S_2

Figure 27. Time development of the centreline velocity normalized with the mean centreline velocity, U_p/U_c. From top to bottom the frequencies are 0.35 Hz, 0.10 Hz and 0.03Hz.

- Wall shear stress, τ_w

The development in time of the wall shear stress, τ_w, over one period is presented in Figure 28 for all three frequencies. The wall shear stress is normalised with its mean value over one period, τ_m. From Figure 28 it can be observed that decreasing the frequency, from 0.35 Hz to 0.03Hz, the numerical simulations results start to have a better estimation of the experimental data for section S_1. At section S_2, the numerical simulations results are deviating from the experimental data with decreasing the frequency.

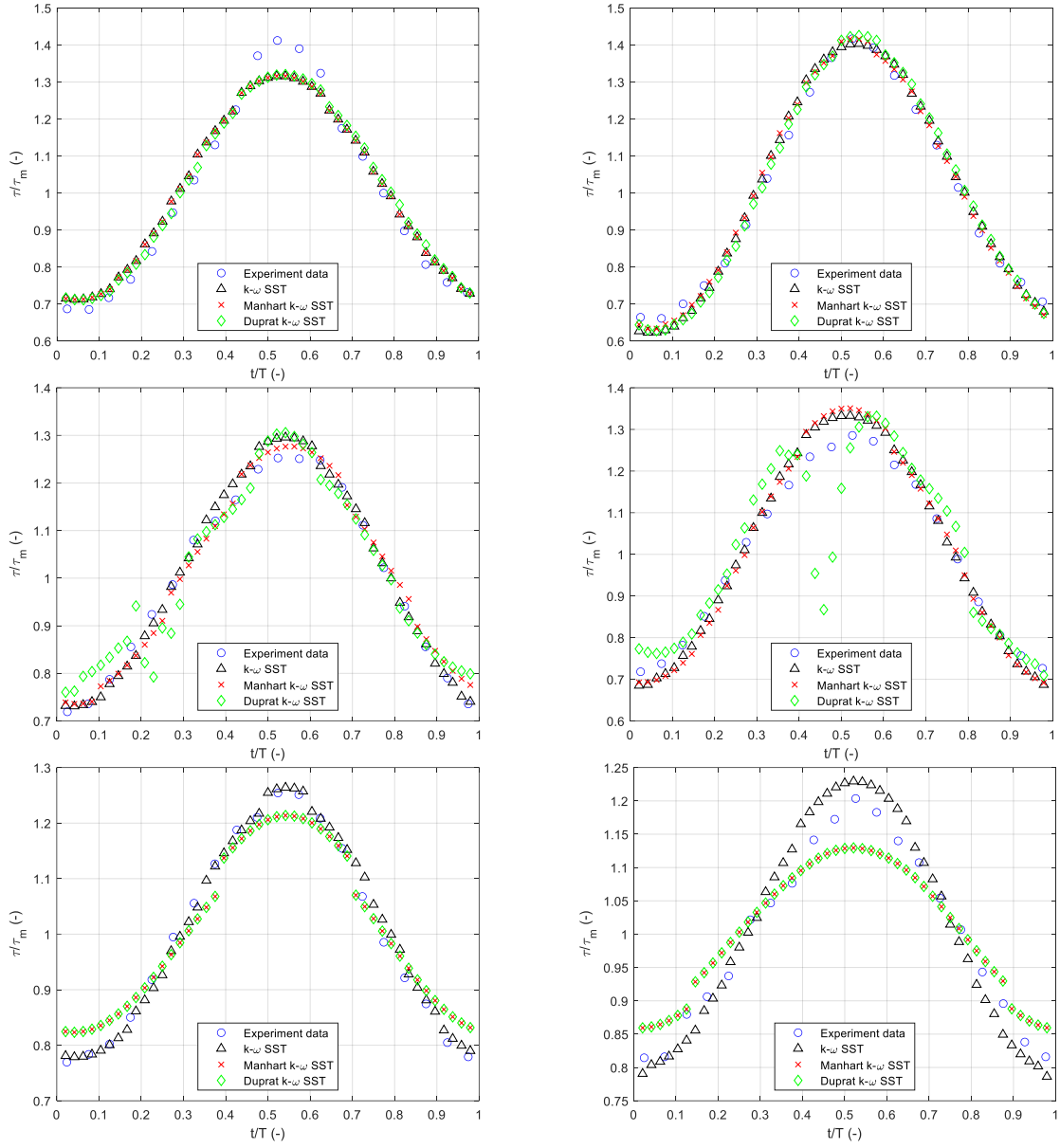

Section S_1 Section S_2

Figure 28. Time development of the wall shear stress, τ_w / τ_m. From top to bottom the frequencies are 0.35 Hz, 0.10 Hz and 0.03Hz.

- **Phased-averaged flow variables**

The phased-averaged quantities used in validating the numerical simulations results are the amplitude of the streamwise oscillating velocity, A_U, and the phase shift of the streamwise velocity oscillations, φ_U. The phased-averaged quantities presented in this section are evaluated over one period, after the periodic convergence was attained.

- Amplitude of the streamwise oscillating velocity, AU

Figure 29 shows the amplitude of the streamwise velocity, A_U, normalised with its value at the centre of the asymmetric diffuser, A_{Uc}, over one period, for all three frequencies. The numerical simulations results are compared with the experimental data and with the Stokes analytical solution for a channel flow [12], at both sections from the diffuser, S_1 and S_2.

The numerical simulations results are in good agreement with the experimental data until the Stokes normal distance, y_s, reaches $y_s = 1$, for all frequencies except for the section S_2 at the 0.35 Hz and 0.03 Hz frequencies. After $y_s = 1$, for the frequency of 0.35 Hz at the section S_1 all the wall models underestimate the maximum amplitude of the experimental data, while at the S_2 section the numerical results are very close to the experimental data. At this frequency

all wall models follow the Stokes solution for both sections, S_1 and S_2. In case of 0.10 Hz frequency, only for the S_2 section the Duprat wall model overestimate the peak values of the experimental measurements while the other wall models, for both sections, have a good estimation of the experiment. The Stokes solution is followed by all wall models until $y_s = 1$. Then the wall models deviate completely from the Stokes solution. For the 0.03 Hz frequency the k-ω SST deviates from the experimental data from $y_s = 0.3$ until $y_s = 5$ where it reaches the centre of the diffuser.

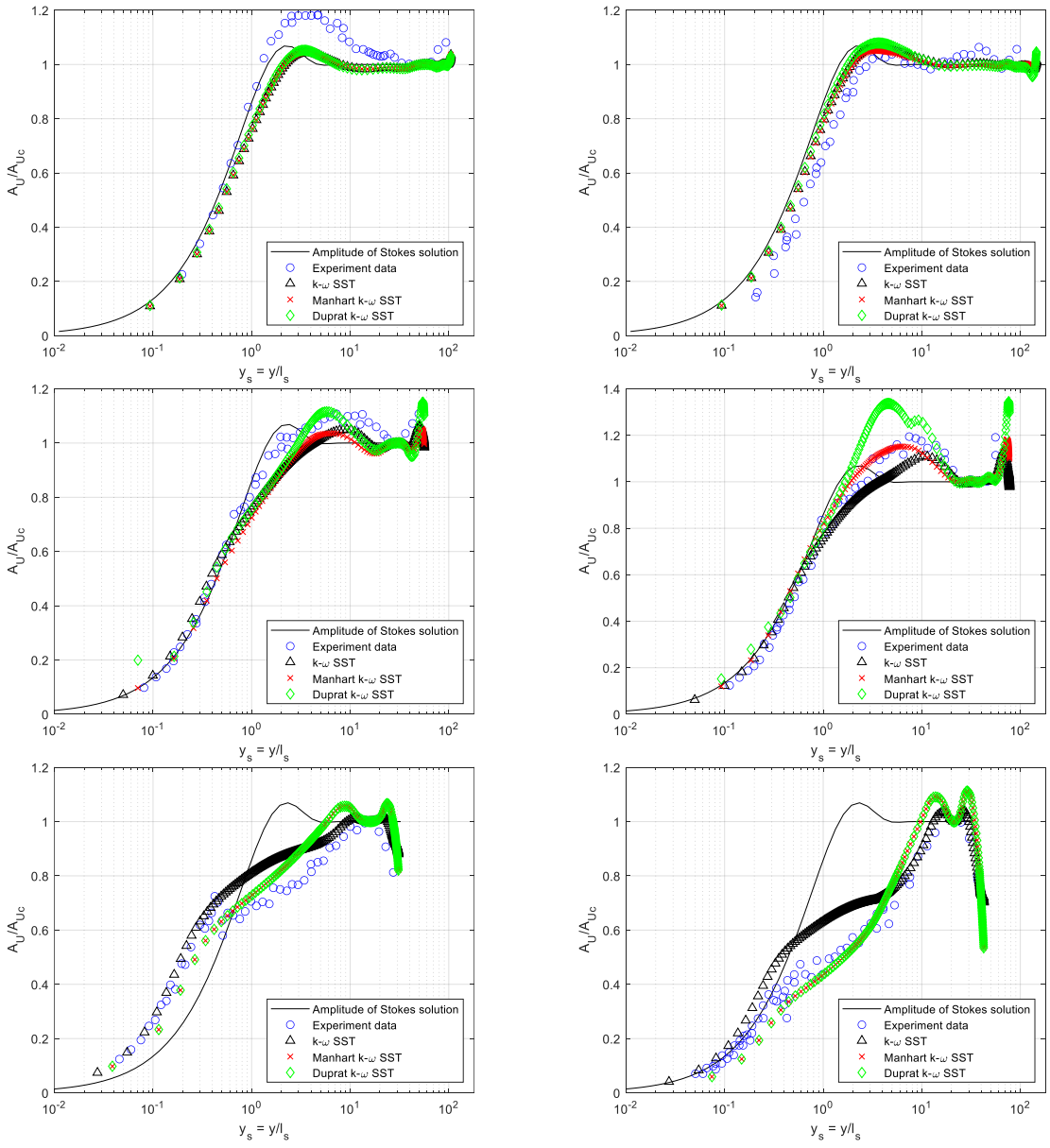

Section S_1 Section S_2

Figure 29. Amplitude of the streamwise oscillating velocity, A_U / A_{Uc}. From top to bottom the frequencies are 0.35 Hz, 0.10 Hz and 0.03Hz.

- Phase shift of the streamwise oscillations, ϕ_U

The phase shift of the streamwise oscillations, ϕ_U, relative to its centre values ϕ_{Uc}, is presented in Figure 30, where the numerical simulations results are validated against the experimental data and the phase of Stokes solution in a channel, for all three frequencies. The phase shift, ϕ_U, from the numerical simulation results was calculated using the equation (26) over one period.

$$\phi = 2\pi f \frac{t}{T} \tag{26}$$

where f is the frequency of the pulsating flows oscillations, t is the time in the oscillation period, and T is the time of oscillation period.

For the frequency of 0.35 Hz all the wall models follow the Stokes solution and until close to the centre of the diffuser, y_s = 10 for section S_1 and y_s = 2 for section S_2, they follow the experimental data also. In the centre of the diffuser the experimental data is underestimated, for section S_1 and overestimated for section S_2. For the other two frequencies, 0.10 Hz and 0.03 Hz, the numerical simulations results deviate completely from the Stokes solution. While approaching to the centre of the diffuser the numerical simulations are showing a good evaluation of the experimental data. The only exception is made by the Manhart and Duprat wall models at the 0.03 Hz frequency in section S_2 where they fail to predict the experimental data almost on the entire diffuser height.

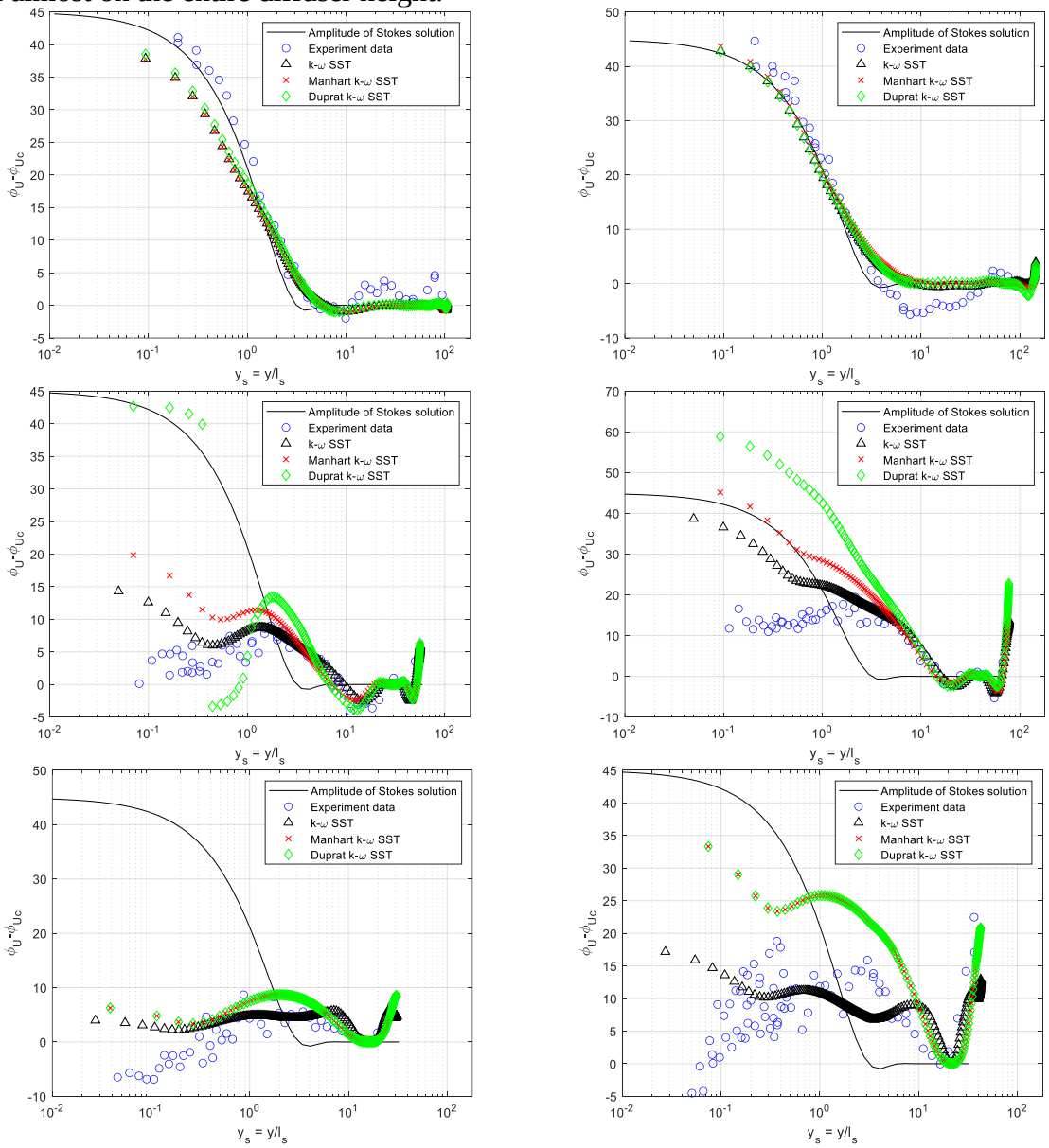

Section S_1 Section S_2

Figure 30. Phase shift of the streamwise oscillations, ϕ_U - ϕ_{Uc}. From top to bottom the frequencies are 0.35 Hz, 0.10 Hz and 0.03Hz.

CONCLUSIONS

In the present thesis numerical studies were carried out of turbulent flows inside an asymmetric diffuser for several flow regimes by using different wall models for estimating the velocity in the near wall region. The flow regimes analysed in the numerical studies are steady-state flow and three pulsating flows with the frequencies of 0.35 Hz, 0.10 Hz and 0.03 Hz. RANS numerical simulations were carried out and the wall models used for predicting the velocity near the wall were the standard formulation of the k - ω SST turbulence model (linear law of the wall), the Manhart wall model [30] and the Duprat wall model [11].

The ***main objective*** of this thesis is to find more economical approaches, i.e., decrease the computational time and effort, for numerical simulations of steady and pulsating flows with strong adverse pressure gradients.

Also, other objectives attained in this thesis are:

- Use of a free, open-source CFD code, Code_Saturne, to perform steady-state and unsteady-state numerical simulations.
- Implement different wall models for estimation of the flow field in the near wall region, Manhart and Duprat wall models, in the CFD solver code to decrease the computational effort required to perform the numerical simulations.
- Perform numerical simulations for both steady flows and unsteady (pulsating) flows using different wall models, built-in wall models (Linear Law of the Wall) and user wall models (Manhart and Duprat).
- Validate the numerical simulations against detailed experimental data, using several flow variables (time-averaged, time-development and phased-averaged flow variables).

The experimental measurements used to validate the numerical simulations presented in this thesis were performed by Cervantes and Engström [12] on an asymmetric diffuser experimental installation located at the Division of Fluid Mechanics, Luleå University of Technology, Luleå, Sweden. The research of this thesis was focused on assessing the performance of recent developments in estimating the near-wall velocity using wall models for steady-state and unsteady-state flows, e.g., pulsating flows, implemented for the first time in RANS turbulence models. Other research investigations were made on the influence over the numerical simulations of the geometry, the mesh domain resolution, the mesh distribution near the wall, the time-step.

The thesis is structured in 9 chapters presented below starting with a general presentation of the actual context for the thesis, followed by the state of the art of wall modelling and the numerical approaches in CFD solvers. The thesis continues with the presentation of the CFD code Code_Saturne, used in carrying out the numerical simulations, followed by the description of the numerical test case and the validation of the numerical results with the experimental data. At the end of the thesis several conclusions and future work directions are presented.

- The present-day context of the electrical grid system stability is presented in the *Introduction chapter*. The Introduction chapter presents the role of the hydropower plants in the stability of the electrical grid system. Also, in this chapter is listed the main numerical approaches and the usual numerical methods focusing on the boundary layer definition. The aim of the thesis is presented in the Introduction chapter considering the limitations of the RANS numerical simulations and methods to decrease the drawbacks of the RANS numerical simulations.
- *Second chapter* presents the state of the art of wall modelling, the common approaches for modelling the flow near the wall. In this chapter the downsides of modelling the wall region are observed given by the mathematical methods or the

computational effort used to perform the numerical simulations. Two wall models are presented in this chapter that endorse the research of the thesis.

- In *the third chapter* the usual numerical approaches used in CFD codes are described, focussing on the economical numerical approaches, i.e., RANS numerical simulations. The wall models of Manhart [30] and Duprat [11] are presented in this chapter, upholding the consideration of the pressure gradient in the estimation of the near wall region flow compared to the standard considerations available in the general literature.
- The CFD code used for conducting the numerical simulations from this thesis is presented in *the fourth chapter*. The CFD code, Code_Saturne, is presented followed by the implementation procedure of wall functions/models approaches in Code_Saturne solver. The chapter first describes how the computation procedure is applied on the flow governing equations and how the computational domain is processed by the Code_Saturne solver. In the second part of the chapter are presented two methods of implementing a wall function or a wall model in the Code_Saturne solver depending on the level of detail the functions modify the CFD solver.
- *The fifth chapter* presents the experimental and numerical setups used in the validation of the numerical simulations results with the experimental data for steady and three pulsating flows. The numerical test cases used in the analyses presented in this thesis are inspired from the experimental case of Cervantes and Engström [12]. The geometry consists of a straight rectangular duct and continues with an asymmetric diffuser. Using ICEM CFD the geometry was prepared for generating the mesh of the numerical test case used in the steady-state and unsteady-state numerical simulations. At the end *the fifth chapter* the boundary conditions and the settings of the numerical simulations are presented.
- In *chapter six* are presented the experimental data obtained by Cervantes and Engström [12], for steady and unsteady (pulsating) flows. The experimental data consist of several flow quantities structured in time-averaged, time-development and phased-averaged quantities.
- The steady-state numerical simulations compared with the experimental data are presented in *chapter seven*, along with the mesh sensitivity studies for the numerical simulations carried out. The numerical simulations were performed using the linear law of the wall, the Manhart [30] and the Duprat [11] wall models. The validation of the steady-state numerical simulations with the experimental data is performed for the time-averaged flow quantities. The time-averaged variables used in the validation of the steady flow numerical simulations are the wall shear stress, τ_w, the friction velocity, u_τ, the dimensionless streamwise velocity U^+, and the dimensionless production of turbulence P_k^+.
- The validation of the unsteady-state numerical simulations with the experimental data is presented in *chapter eight*. The sensitivity studies carried out for the unsteady numerical simulations are presented at the beginning of the chapter based on the Stokes second problem case. The numerical simulations were performed using the three wall models also used for the steady-state numerical simulations. The unsteady-state numerical simulations were carried out for three pulsating turbulent flows based on following oscillation frequencies: 0.03 Hz, 0.10 Hz, and 0.35 Hz. The validation of the unsteady-state numerical simulations with the experimental data are presented structured in three parts: time-averaged flow variables (dimensionless streamwise velocity U^+ and dimensionless production of turbulence P_k^+), time-development flow variables (centreline diffuser velocity, U_p, and wall shear stress, τ_w), and phased-averaged flow variables (amplitude of the streamwise oscillating velocity, A_U, and phase shift of the streamwise oscillations, φ_U).

- At the end of the thesis, in *the nineth chapter*, several conclusions and future work directions are presented along with the personal contributions to the thesis by the author.

General conclusions

For reaching the main objective of the present thesis, i.e., to decrease the computational time and effort of numerical simulations using wall models in pulsating flows with strong adverse pressure gradients, two concepts have been studied.

First, for any kind of turbulent flow, the boundary layer was investigated. Different wall models were implemented and validated against experimental measurements of flows in geometries that are affected by the adverse pressure gradient. One of the most important parameters of the boundary layer in numerical simulations was the dimensionless distance from the wall to the first computational point, y^+. Depending on the numerical method used, e.g., wall model, turbulence model etc., the computational domain, i.e., the mesh of the numerical simulation, requires different mesh distributions.

Second, in the case of turbulent pulsating flows, the oscillating layer of the flow was investigated. The parameter that defines the oscillating layer of the pulsating flows is the height of the oscillating layer, δ_s. Because the pulsating flows represent a special case in turbulent flows, to properly prepare a numerical simulation of a pulsating flow two parameters need to be taken in consideration and find the most restrictive parameter to model. The parameters that are important in order to run a numerical simulation are the y^+ and the δ_s, and they need to be modelled from the first stages of the numerical simulation that is the mesh generation step. For successfully run a numerical simulation of a pulsating flow the oscillating layer requires a certain mesh discretization, as seen in chapter 8, to capture the effects of the flow pulsations. Often the mesh discretization of the oscillating layer is more restrictive to the size of the mesh cell than the boundary layer mesh discretization. At fast oscillating frequencies, e.g., 0.35 Hz and 0.10 Hz, the cell size of the oscillating layer is smaller than the cell size of the boundary layer.

Therefore, the first step in reaching the goal of the thesis, was to prepare the geometry for which the mesh will be generated for the numerical simulations presented in this thesis. From the experimental setup presented in Cervantes and Engström [12] was kept the straight rectangular duct followed by an asymmetric diffuser in which the top wall of the diffuser is diverging. All the irregularities of the geometry, like discontinuities and multiples instances of the elements of the geometry, were corrected in order to generate on a smooth geometry a good mesh quality domain. Bringing the geometry of the asymmetric diffuser to a high quality, the criteria for the boundary layer, y^+, and oscillating layer were successfully attained accordingly to the turbulence models and pulsating flow phenomena requirements. The sensitivity analyses were carried out for each numerical simulation of each wall model in order to find the appropriate mesh, time-step and the time needed for running the numerical simulations, i.e., number of periods of the pulsating flow. The mesh refinement procedure was performed using the guidelines from Celik et al. [31]. The mesh domain used in the numerical simulations presented in this thesis was prepared in the ANSYS ICEM CFD tool.

The performance of the wall models results presented in this thesis was assessed using steady-state and unsteady-state RANS numerical simulations. The unsteady-state numerical simulations were carried out for three frequencies: 0.35 Hz, 0.10 Hz and 0.03 Hz.

The steady-state numerical simulations were performed on the full geometry of the asymmetric diffuser using as the initial conditions the mean variables of the flow. The numerical analyses were carried out using a free open source CFD toll called Code_Saturne. The domain used for numerical analyses was comprised from the straight rectangular duct followed by the asymmetric diffuser. To model the velocity in the boundary layer three wall

models were employed: the standard formulation of the k-ω SST turbulence model (linear law of the wall), the Manhart wall model and the Duprat wall model. Compared to the standard k-ω SST turbulence model the Manhart and Duprat wall models allow the use of a coarser mesh discretization leading to faster numerical results without compromising the accuracy of the results. All the numerical simulations were performed using the k-ω SST turbulence model.

To verify the implementation of the Manhart and Duprat wall models a double validation of the numerical simulation results was performed. The results of the Manhart and Duprat wall models were firstly validated against the results of the standard k-ω SST turbulence model and after another validation was performed against the experimental measurements. The experimental data were obtained using LDA techniques in two sections of the asymmetric diffuser. One section, at section S_1 (x = 2.082 m), located just before the beginning of the asymmetric diffuser and the other section, at section S_2 (x = 2.632 m), located close to the curvature of the asymmetric diffuser.

The validation of the steady-state numerical results was performed on the time-averaged variables of the flow: the dimensionless streamwise velocity U^+ and the dimensionless production of the turbulence kinetic energy P_k^+. The averaged variables used in the validation process of the wall models and the experimental measurements were extracted from the two sections of the geometry. Comparing the numerical results from the three wall models with the experimental data showed an underestimation of the variables used for validation. The three wall models showed a good approximation of the experimental data in the case of the streamwise velocity, U^+, in the near wall region but getting away from the wall the results start to diverge from the experimental data. In the case of the production of the turbulence kinetic energy, P_k^+, the results from the wall models follow the trend of the experimental data but the wall models deviate completely from the experimental data on the entire height of the diffuser. The time required to complete the numerical simulations was approximately equally for all the wall models to around 3 hours with a sightly decrease in simulation time for the Manhart and Duprat wall models.

The behaviour of the pulsating flows was investigated by performing unsteady-state RANS numerical simulations for three oscillating frequencies of 0.35 Hz, 0.10 Hz and 0.03 Hz. For each oscillation frequency three unsteady-state numerical simulations were carried out using the same wall models that were applied for the steady-state numerical simulations: the linear law of the wall, the Manhart wall model and the Duprat wall model. The settings of the pulsating flows numerical simulations were defined to resemble the experimental procedure. Therefore, the variable of interest in carrying out the numerical simulations was the experimental flow rate from which it was imposed the average velocity at the inlet of the numerical test case. The validation procedure of the numerical simulations of the pulsating flows was carried out against experimental measurements performed using LDA techniques. To induce the oscillations of the pulsating flows a cosine function of the velocity at the inlet boundary condition was imposed. Several tests were performed on the inlet boundary condition by including a perturbation in the amplitude of the inlet velocity profile to match the results of the numerical simulations to the experimental measurements. The unsteady-state numerical simulations, due to the restrictions of the CFD tool Code_Saturne, were carried out using a velocity profile rather than a steady-state numerical simulation as the usual CFD tools require.

In order to perform an unsteady-state numerical simulation of a pulsating flow the mesh discretisation near the wall needs to be refined depending on the oscillation frequency. As observed in chapter 6 the height of the oscillating layer decrease with the increase of the oscillation frequency leading to a small cell height near the wall. Therefore, the region near the wall requires a high refinement of the mesh discretisation resulting in an increase in the computational effort to perform the numerical simulations. To reduce the computational effort of the numerical simulations and due to the symmetry of the asymmetric diffuser test case it was possible to use only half of the considered geometry used in the steady-state numerical simulations.

In order to use the proper settings for the numerical simulations of the asymmetric diffuser a simple case of an oscillating flat plate, the Stokes 2nd problem, was investigated for all three frequencies. For each oscillating frequency mesh and time-step sensitivity analyses were performed for the test case of Stokes 2nd problem. The results of the sensitivity analyses were compared with the exact solution of the Stokes 2nd problem therefore to accurately represent the pulsating behaviour of the pulsating flows several configurations are required. Regarding the mesh configuration the mesh sensitivity analyses showed that the oscillating layer should consists of at least 50 cell layers. From the time-step sensitivity analyses resulted that for a good representation of the oscillations of the pulsating flows it was necessary a time-step that leads to at least 40 points per oscillation period and the Courant-Friedrichs-Lewy (CFL) condition should be below 50. The mesh discretisation and time-step resulted from the Stokes 2nd problem cases were applied to the numerical simulations of the asymmetric diffuser test cases.

The validation of the unsteady-state numerical simulations results of the Manhart and Duprat wall models were carried out against the numerical simulations of the standard formulation of the k-ω SST turbulence model and the experimental data. The validation of the unsteady-state numerical simulations was performed for three categories of flow variables: time-averaged (dimensionless streamwise velocity U^+ and dimensionless production of turbulence P_k^+), time-development (centreline diffuser velocity, U_p, and wall shear stress, τ_w), and phased-averaged (amplitude of the streamwise oscillating velocity, A_U, and phase shift of the streamwise oscillations, φ_U). The results of the wall models showed a very good approximation of the experimental data for the time-development flow variables for the entire range of the data points. In the case of the time-averaged and phased-averaged flow variables the wall models fail in estimating the experimental measurements over the entire spectrum of data points. The time-averaged variables are better estimated near the wall and the phased-averaged variables are better estimated in the centre of the asymmetric diffuser. A reason for this behaviour is that all three wall models presented in this thesis are developed for the mean flow which occur in the centre of the asymmetric diffuser. The phased-averaged flow variables were compared, in addition to the experimental data, with the Stokes solution for a laminar channel flow. The wall models show a good approximation of the Stokes solution in the centre of the asymmetric diffuser where the mean flow occurs but in the near wall region the wall models fail to approximate the Stokes solution. The Stokes solution is approximated better than the experimental data by the wall models over the entire diffuser height in both sections at high frequencies and the results of the Manhart wall model are the closest to the Stokes solution than the other wall models. For the 0.10 Hz frequency the Duprat wall model fails to estimate the experimental data and the Stokes solution except for the time-averaged variables. The cause might be the instabilities of the 0.10 Hz pulsating flow frequency that generated in the Code_Saturne solver. When the 0.10 Hz numerical simulation was carried out with the Duprat wall model was observed a struggle in convergence stability of the Code_Saturne solver. The differences in the results of the wall models numerical simulations and the experimental data might come from the assumptions made to develop the wall models, since the wall models were developed from the estimation of the mean flow parameters. Therefore, some modifications are required for the wall models presented in this thesis in order to attain a better estimation of the flow in the case of an unsteady-state numerical analysis.

Another important aspect of performing unsteady-state numerical simulations is the amount of time a numerical simulation takes to reach the convergence state. Comparing the numerical simulations, the Manhart and Duprat wall models showed a decrease in the required time with at least several hours in the case of the 0.35 Hz frequency up to several days in the case of 0.03 Hz frequency. An exception in the decreasing of simulation time was observed in the case of 0.10 Hz only for the Duprat wall model. A cause to the large simulation time generated by the Duprat wall model might by due to the instabilities generated by the pulsating flow in the Code_Saturne solver.

The comparisons of the numerical simulations carried out using the Manhart and Duprat wall models showed that they are viable, more economical, and can be considered alternatives to the already implemented wall models with negligeable loss in accuracy. The main advantage of the Manhart and Duprat wall models is the use of a coarser mesh distribution, up to a $y^+ = 5$. The ability to use a coarser mesh distribution is due to the involving of more flow parameters in the prediction of the flow in the near wall region. The Manhart and Duprat wall models consider, more than the standard wall model formulation of the k-ω SST turbulence model, the streamwise pressure gradient which represent an important parameter of the flow.

Personal contributions

Performing steady-state or unsteady-state numerical simulations has become more and more available to the average computers for simple cases but it is difficult to obtain fast and accurate results of the complex turbulent flows, e.g., pulsating flows. Furthermore, the use of new mathematical expressions, other than the already implemented ones, requires a high amount of knowledge of the programming language/s of the CFD solver code and time for testing and validate the results of the numerical simulations.

The original work presented in this thesis is summarized in the following points:

- Prepare the geometry for generating the mesh discretization domain for the numerical test cases presented in this thesis. To generate a high quality mesh the geometry used in the numerical analysis must be complete without any gaps and overlapped elements, e.g., lines, points etc.
- Generate the mesh discretisation domain further used for the numerical simulations. A higher mesh quality is preferable to obtain high quality numerical simulations results. The mesh quality is verified using the mesh quality criteria available in the mesh generation software and they should correspond with the mesh quality criteria verified by the CFD solver. The mesh was generated at first as a structured mesh and in the final stage of mesh generation it was converted in unstructured mesh for a better alignment of the geometry particularities and curvature. Depending on the flow modelled, steady flow or pulsating flow, the boundary layer or the oscillating layer were discretized accordingly to capture the flow particularities while minimizing the computational effort.
- Develop the implementation procedure of the Manhart and Duprat wall models required by the CFD solver Code_Saturne. To perform the implementation of the Manhart and Duprat wall models in the Code_Saturne solver, the knowledge of several programming languages was necessary, e.g., Fortran90, C and C++. Also, the internal functions of the Code_Saturne solver were analysed to establish a strong and fast connection between the results of the wall models and the core of the Code_Saturne solver.
- Investigate the implementation of the Manhart and Duprat wall models in the Code_Saturne solver for several test cases. The validation of the implementation procedure for the Manhart and Duprat wall models were performed starting from simple cases up to more complex test cases. The simple cases were represented by a flow over a flat plate, flow in a plane channel and the flow in a straight pipe. The complex test cases are a flow in a pipe with converging and diverging designs and a flow in an asymmetric diffuser with small adverse pressure gradient other than the one presented in this thesis.
- Perform RANS steady-state numerical simulations on the asymmetric diffuser numerical test case and validate those results against experimental data using time-averaged variables. For the steady-state numerical simulations mesh sensitivity analyses were carried out to reduce the computational effort while preserving a good

approximation of the numerical simulations results when comparing with the experimental data.

- Develop, for the numerical simulations of pulsating flows, a relationship between the boundary layer and the oscillating layer to model near wall region using the Stokes 2nd problem.
- Analyse the influence of the inlet boundary condition for the unsteady-state numerical simulations to accurately analyse the behaviour of the pulsating flows.
- Perform RANS unsteady-state numerical simulations for three frequencies (0.35 Hz, 0.10 Hz and 0.03 Hz) on the asymmetric diffuser numerical test case.
- Validate the results of the unsteady-state numerical simulations against experimental data using time-averaged, time-development and phased-averaged variables. To obtain the best equilibrium between the accuracy of the numerical results and the computational effort was used the Stokes 2nd problem test case for all three frequencies. For the stokes 2nd problem were conducted mesh sensitivity analyses and time step sensitivity analyses, and the results of the sensitivity analyses were used on the asymmetric diffuser test case presented in this thesis.

Future work

The research work presented in this thesis will be continued further to validate and improve the wall models of Manhart and Duprat, in both steady-state and unsteady-state numerical simulations.

The Manhart and Duprat wall models will be tested on a coarser mesh discretisation where the dimensionless distance to the wall, y^+, is greater than 5. A coarser mesh can lead to faster numerical simulations and to other comparisons of the Manhart and Duprat wall models, e.g., with the Standard Wall Function.

An improvement in developing the Manhart and Duprat wall models will be to further optimize the calculus algorithms of the wall models in order to perform faster numerical simulations.

Another improvement of the Manhart and Duprat wall models will be performed by adding more flow parameters, e.g., the roughness of the walls, to increase the accuracy of the wall models or by decrease the computational effort.

Other type of numerical simulations can be performed using the Manhart and Duprat wall models such as to carry out LES based numerical simulations or hybrid RANS - LES numerical simulations in more complex geometries as a hydraulic turbine.

An important future aim is testing the Manhart and Duprat wall models in more complex geometries with flows with a high degree of turbulence, such as the flow in a hydraulic turbine draft tube (Francis99 NTNU) or even in the entire domain of a hydraulic turbine, from the inlet of the spiral casing to the outlet of the draft tube.

REFERENCES (SELECTION)

[1] IEA - International Energy Agency, “Energy Statistics Data Browser,” IEA, 22 September 2022. [Online]. Available: https://www.iea.org/data-and-statistics/data-tools/energy-statistics-data-browser. [Accessed 2022].

[2] K. Amiri, M. J. Cervantes and B. Mulu, “Experimental investigation of the hydraulic loads on the runner of a Kaplan turbine model and the corresponding prototype,” *Journal of Hydraulic Research,* vol. 53, no. 4, 2015.

[3] T. Chirag, G. Bhupendra and M. Cervantes , “Effect of transients on Francis turbine runner life: a review,” *Journal of Hydraulic Research,* vol. 51, no. 2, pp. 121-132, 2013.

[4] B. Mulu, An experimental and numerical investigation of a Kaplan turbine model (Ph. D. Thesis), Luleå: Luleå tekniska universitet, 2012.

[5] H. Keck and M. Sick, "Thirty years of numerical flow simulation in hydraulic turbomachines," *Acta Mechanica,* vol. 201, no. 1, pp. 211-229, 2008.

[6] J. H. Ferziger and M. Perić, Computational Methods for Fluid Dynamics, Springer Berlin Heidelberg, 2002.

[7] S. Pope, Turbulent Flows, Cambridge: Cambridge university Press., 2000.

[8] M. Manhart, N. Peller and C. Brun, “Near-wall scaling for turbulent boundary layers with adverse pressure gradient,” *Theoretical and Computational Fluid Dynamics,* vol. 22, no. 3-4, 2008.

[9] C. Duprat, G. Balarac, O. Métais, P. M. Congedo and O. Brugière, “A wall-layer model for large-eddy simulations of turbulent flows with/out pressure gradient,” *Physics of Fluids,* vol. 23, no. 1, 2011.

[10] C. Duprat, “Simulation numérique instationnaire des écoulements turbulents dans les diffuseurs des turbines hydrauliques en vue de l’amélioration des performances”, Ph.D. dissertation, Grenoble: Institut National Polytechnique de Grenoble – INPG, Laboratoire des Écoulements Géophysiques et Industriels, 2010.

[11] C. Duprat, Simulation numérique instationnaire des écoulements turbulents dans les diffuseurs des turbines hydrauliques en vue de l’amélioration des performances, Ph.D. dissertation, Grenoble: Institut National Polytechnique de Grenoble – INPG, Laboratoire des Écoulements Géophysiques et Industriels, 2010.

[12] M. J. Cervantes and T. F. Engström, “Pulsating turbulent flow in a straight asymmetric diffuser,” *Journal of Hydraulic Research,* vol. 46, no. SUPPL. 1, 2008.

[13] S. Salehi, M. Raisee and M. J. Cervantes, “Computation of developing turbulent flow through a straight asymmetric diffuser with moderate adverse pressure gradient,” *Journal of Applied Fluid Mechanics,* vol. 10, no. 4, 2017.

[14] J. Ohlsson, P. Schlatter, P. F. Fischer and D. S. Henningson, “Direct numerical simulation of separated flow in a three-dimensional diffuser,” *Journal of Fluid Mechanics,* vol. 650, 2010.

[15] P. E. Smirnov and F. R. Menter, “Sensitization of the SST turbulence model to rotation and curvature by applying the Spalart-Shur correction term,” *Journal of Turbomachinery,* vol. 131, no. 4, 2009.

[16] S. Jakirlić, G. Kadavelil, M. Kornhaas, M. Schäfer, D. C. Sternel and C. Tropea, “Numerical and physical aspects in LES and hybrid LES/RANS of turbulent flow separation in a 3-D diffuser,” *International Journal of Heat and Fluid Flow,* vol. 31, no. 5, 2010.

[17] N. Maheu, V. Moureau, P. Domingo, F. Duchaine and G. Balarac, “Large-eddy simulations of flow and heat transferaround a low-Mach number turbine blade,” in *Center for Turbulence Researc, Proceedings of the Summer Program,* 2012.

[18] M. Manhart and R. Friedrich, “DNS of a turbulent boundary layer with separation,” *International Journal of Heat and Fluid Flow,* vol. 23, no. 5, 2002.

[19] S. Hosseini, R. Vinuesa, P. Schlatter, A. Hanifi and D. Henningson, “Direct numerical simulation of the flow around a wing section at moderate Reynolds number,” 2016.

[20] C. Baker, T. Johnson, D. Flynn, H. Hemida, A. Quinn, D. Soper and M. Sterling, “Computational techniques,” Elsevier, 2019.

[21] A. Leonard, “Energy cascade in large-eddy simulations of turbulent fluid flows,” 1974.

[22] ANSYS Inc., ANSYS® Academic Research, Release 16.2, Help System, Fluent Theory Manual.

[23] Code Saturne, *Code Saturne Theory Guide 5.0.9,* Paris: EDF R&D, 2018.

[24] ANSYS Inc., ANSYS® Academic Research, Release 16.2, Help System, CFX Theory Manual.

[25] R. L. Simpson, “A model for the backflow mean velocity profile,” 1983.

[26] C. Duprat, O. Métais and G. Balarac, “Large Eddy simulation of a high Reynolds number swirling flow in a conical diffuser,” in *ERCOFTAC Series,* 2010.

[27] ANSYS Inc., ANSYS® Academic Research, Release 16.2, Help System, ICEM CFD Theory Manual.

[28] Code_Saturne, Code Saturne Theory Guide 5.0.9, Paris: EDF R&D, 2018.

[29] M. M. Gibson and B. E. Launder, “Ground effects on pressure fluctuations in the atmospheric boundary layer,” *Journal of Fluid Mechanics,* vol. 86, no. 3, pp. 491-511, 6 1978.

[30] M. Manhart, N. Peller and C. Brun, “Near-wall scaling for turbulent boundary layers with adverse pressure gradient,” *Theoretical and Computational Fluid Dynamics,* vol. 22, no. 3-4, 2008.

[31] I. B. Celik, U. Ghia, P. J. Roache and C. J. Freitas, “Procedure for Estimation and Reporting of Uncertainty Due to Discretization in CFD Applications,” ASME J. Fluids Eng, 2008.